

Detecting Earth's Temporarily-Captured Natural Satellites — Minimoons

Bryce Bolin^{1,2} (bolin@ifa.hawaii.edu), Robert Jedicke¹, Mikael Granvik³, Peter Brown⁴,
Ellen Howell⁵, Michael C. Nolan⁵, Peter Jenniskens⁶, Monique Chyba⁷, Geoff Patterson⁷,
Richard Wainscoat¹

Received December 22, 2013; accepted May 20, 2014

44 Pages, 14 Figures, 1 Table

¹University of Hawaii, Institute for Astronomy, 2680 Woodlawn Dr, Honolulu, HI, 96822

²University of Phoenix, Hawaii Campus, 745 Fort St, Honolulu, HI 96813

³Department of Physics, P.O. BOX 64, 00014 University of Helsinki, Finland

⁴University of Western Ontario, Physics & Astronomy Department, London, Ontario,
Canada

⁵Arecibo Observatory, Arecibo, Puerto Rico

⁶SETI Institute, Carl Sagan Center, 189 Bernardo Avenue, Mountain View, CA 94043

⁷University of Hawaii, Department of Mathematics, Honolulu, HI, 96822

ABSTRACT

We present a study on the discoverability of temporarily captured orbiters (TCOs) by present day or near-term anticipated ground-based and space-based facilities. TCOs (Granvik *et al.* 2012) are potential targets for spacecraft rendezvous or human exploration (Chyba *et al.* 2014) and provide an opportunity to study the population of the smallest asteroids in the solar system. We find that present day ground-based optical surveys such as Pan-STARRS and ATLAS can discover the largest TCOs over years of operation. A targeted survey conducted with the Subaru telescope can discover TCOs in the 0.5 m to 1.0 m diameter size range in about 5 nights of observing. Furthermore, we discuss the application of space-based infrared surveys, such as NEOWISE, and ground-based meteor detection systems such as CAMS, CAMO and ASGARD in discovering TCOs. These systems can detect TCOs but at a uninteresting rate. Finally, we discuss the application of bi-static radar at Arecibo and Green Bank to discover TCOs. Our radar simulations are strongly dependent on the rotation rate distribution of the smallest asteroids but with an optimistic distribution we find that these systems have $> 80\%$ chance of detecting a > 10 cm diameter TCO in about 40 h of operation.

Subject headings: Near-Earth Objects; Asteroids; Dynamics

Proposed Running Head: Detecting Earth’s Natural Satellites

Editorial correspondence to:

Bryce Bolin

Institute for Astronomy

University of Hawaii

2680 Woodlawn Drive

Honolulu, HI 96822

Phone: +1 808 294 6299

Fax: +1 808 988 2790

E-mail: bolin@ifa.hawaii.edu

1. Introduction

Granvik *et al.* (2012) suggested that there exists a steady state population of natural irregular satellites of the Earth. We will call these objects temporarily captured orbiters (TCO) or minimoons. There is almost no previous work on TCOs and what little exists is reviewed in Granvik *et al.* (2012). They are captured from a dynamically suitable subset of the near-Earth object (NEO) population — those that are on Earth-like orbits with semi-major axis $a \sim 1.0$ AU, eccentricity $e \sim 0.0$ and inclinations $i \sim 0$ deg — and complete an average of ~ 2.9 revolutions around Earth during their average capture duration of about 290 days or 9.5 months. In this work we evaluate options for detecting the TCOs as they are being captured, while they are on their geocentric trajectories, and in their meteor phase (about 1% of TCOs enter Earth’s atmosphere).

The first confirmed TCO, 2006 RH₁₂₀, was discovered in 2006 by the Catalina Sky Survey (Larson *et al.* 1998; Kwiatkowski *et al.* 2009). Its pre- and post-capture orbit, geocentric trajectory, size, and TCO lifetime were consistent with the Granvik *et al.* (2012) model (that did not include information about 2006 RH₁₂₀). 2006 RH₁₂₀ had an absolute magnitude of $H = 29.9 \pm 0.3$ corresponding to a diameter in the range of 2 to 6 meters if we assume S- and C-class albedos (p_v) of 0.26 and 0.064 respectively (Mainzer *et al.* 2012). This size range is consistent with the preliminary estimate of > 2.3 m diameter from the Goldstone radar facility¹. For comparison, Granvik *et al.* (2012) suggest that the largest TCO in the steady state population is in the 1 to 2 m diameter range, that objects in the 5 to 10 m diameter range are captured every decade, and a 100 m diameter TCO is captured about every 100,000 years. Thus, the predicted flux of objects in 2006 RH₁₂₀’s size range is in rough agreement with the length of time that optical telescopic surveys have been in regular operation and their time-averaged sensitivity to objects like 2006 RH₁₂₀.

¹L. Benner, personal communication.

However, there is no *a priori* reason to expect that the actual TCO orbit and size-frequency distribution (SFD) should match the Granvik *et al.* (2012) model because they used the Bottke *et al.* (2002) NEO orbit model that is strictly applicable only to much larger objects of $\gtrsim 100$ m diameter and made no allowance for non-gravitational forces acting on the small NEOs (*e.g.* the Yarkovsky effect Morbidelli and Vokrouhlický 2003). Granvik *et al.* (2012)’s favored TCO SFD from Brown *et al.* (2002) for bolides is appropriate for TCOs in the 0.1 cm to 1 m diameter range but the TCO orbit distribution should be considered suspect without accounting for the radiation forces.

Furthermore, the orbit distribution from the Bottke *et al.* (2002) NEO model has several known problems including but not limited to 1) underestimating the fraction of the NEO population with perihelion $q < 1.0$ AU, 2) underestimating the fraction of objects on low inclination orbits (Greenstreet and Gladman 2012) and 3) having coarse resolution in (a,e,i)-space. These issues are particularly important because they make it difficult to estimate the population of dynamically capturable NEOs. For instance, the entire set of pre-capture TCO orbits is contained within just 4 bins in the Bottke *et al.* (2002) NEO model. Thus, measuring the TCO size and orbit distribution provides a sensitive means of testing current NEO and meteoroid SFD models in a size range that transitions between the two regimes.

The problem with discovering and characterizing the smallest NEOs is that they are discovered close to Earth when they are moving so fast that there is almost no time to coordinate followup during the time when they are brightest. The smallest known NEO with $H \sim 33.2$ (2008 TS₂₆; Boattini *et al.* 2008) corresponds to a sub-meter diameter meteoroid². The smallest NEO with a measured period is 2006 RH₁₂₀, and the smallest

²To facilitate the conversion between absolute magnitude and diameter we use an albedo of $p_v \sim 0.11$ throughout this work. This albedo results in a 1 km diameter object with

NEO with measured colors/spectrum is 2008 TC₃ (Jenniskens *et al.* 2009), the first object that was discovered prior to impact. TCOs offer an opportunity to obtain good physical characterization of small asteroids because some will be visible for days or weeks and their location can be predicted accurately. Measuring their spin rates over a long temporal baseline may enable a determination of the YORP effect (*e.g.* Bottke *et al.* 2006) and/or the detection of the change in an asteroid’s spin properties during close and slow Earth encounters (*e.g.* Moskovitz *et al.* 2013). Additionally, their taxonomic classification will have implications for the relative delivery rates of objects in this size range from the main belt (*e.g.* Bottke *et al.* 2002).

Pre-impact observations of impactors has value extending beyond improving asteroid-meteorite linkages as exemplified by the case of 2008 TC₃ (Jenniskens *et al.* 2009) and the Almahatta Sitte meteorite (Jenniskens *et al.* 2010). More generally, since all observations of meteoroids impacting Earth use the atmosphere as a detector, there is an urgent need for calibration, particularly of mass, across all meteor measurement techniques. This is a challenging problem as the physical nature of the meteoroid prior to impact is almost always unknown (2008 TC₃ being the one exception). Attempts to calibrate the optical meteoroid mass scale in the 1960s using gram-sized artificial meteors (Ayers *et al.* 1970) were limited to disk or cone-shaped pure iron-nickel materials for operational simplicity, which limited their applicability to the question of pre-atmospheric masses of highly porous, randomly shaped, non-iron meteoroids. No similar artificial meteor measurements have been performed for any other measurement technique (*e.g.* radar meteor calibration).

$H = 18$, a 1 m diameter has $H = 33$, and a 10 cm diameter object has $H = 38$. Our choice makes a difference of only about 13% in the calculated diameter at any absolute magnitude relative to the ‘usual’ assumption of $p_v = 0.14$ — well below the systematic error in the NEO and TCO models and the systematic errors intrinsic to our TCO SFD assumption

Natural meteorites have been used to calibrate the mass of their parent meteoroids for ~ 20 fireballs (*e.g.* Brown *et al.* 2011; Popova *et al.* 2011) but the technique (Ceplecha and Revelle 2005) is only applicable to meteoroids with masses of tens of kilograms.

TCOs could provide the calibration standards if enough of them can be discovered because 1% of them eventually become low-speed meteors (Granvik *et al.* 2012). As the impact location of a TCO would be known in advance, ground deployment of suitable sensors could be undertaken allowing for meteoroid-meteor calibration campaigns. Moreover, knowledge of the shape and rotation state of a TCO prior to impact could help resolve the ongoing debate over whether time-varying optical meteor emission (*e.g.* Beech and Brown 2000) and received radar power (Kero *et al.* 2005) is due to meteoroid rotation modulating ablation or some other mechanism (Babadzhanov and Konovalova 2004).

Finally, TCOs are likely the lowest Δv natural targets for spacecraft missions (Granvik *et al.* 2013, 2012; Elvis *et al.* 2011). The opportunity to retrieve kilograms or even hundreds of kilograms of pristine asteroidal material unaffected by passage through Earth’s atmosphere and uncontaminated by exposure to elements on Earth’s surface would be a tremendous boon to solar system studies. We can even imagine multiple retrieval missions to TCOs that have been taxonomically pre-classified as interesting targets — essentially sampling the range of the main belt in our own backyard.

2. Observable characteristics of the steady state TCO population

Granvik *et al.* (2012) provide trajectories (orbits) for about 18,000 TCOs that are designed to be a representative, unbiased, population. We have used this synthetic TCO population to calculate the observable properties of the steady state TCO population as described in detail in the appendix.

Geocentric TCO spatial distribution

Fig. 1 is useful for understanding the observable characteristics of TCOs with special relevance to their detection by radar or spacecraft. Note that there are high TCO density patches near the Sun-Earth L1 and L2 points and also at 4 LD (lunar distance, ~ 0.00257 au) in the direction towards east and west quadrature. The largest steady-state TCOs are just barely visible at opposition at this distance even with large aperture ground-based visible light surveys. Their overall spatial distribution from this viewpoint is oval with the elongation perpendicular to the Sun-Earth direction. Some of the minimoons can extend to just beyond 10 LD in the direction of both quadratures. The magnified distribution in the right panel shows an enhancement of objects at the Moon’s distance with a ‘moat’ in the density at ~ 1.5 LD. There is also an enhancement of TCOs near Earth at the quadratures — while the TCOs may be close to Earth in this orientation their phase angle will be $\sim 90^\circ$ and they will appear much fainter in visible light than at the same distance in the direction towards opposition. Unfortunately, the TCOs are depleted in the anti-Sun direction out to and beyond the Moon’s distance.

The TCO geocentric distance distribution illustrated in fig. 2 is critical to assessing opportunities for detecting and even discovering TCOs at radar facilities (see §5). There is no significant difference between the distributions in the L1 and L2 directions or in the east and west quadratures but there is a clear difference between the two sets. The average geocentric distance is $4.3 \pm 2.2(\text{rms})$ LD for the L1/L2 regions, $5.7 \pm 2.9(\text{rms})$ LD for the regions near the east and west quadratures, and $4.1 \pm 1.6(\text{rms})$ LD for the entire TCO population. The differences work in favor of optical detection of the TCOs since they are closer to Earth near opposition but a 1 m diameter object with absolute magnitude $H \sim 33$ will have an apparent magnitude of $V = 23.1$ at the average opposition distance. The peaks at ~ 0.5 and ~ 1.5 LD are caused by long-lived particles that have lifetimes of $> 2,000$ d.

Geocentric TCO sky plane distribution

Granvik *et al.* (2012) provide trajectories (orbits) for about 18,000 TCOs that are designed to be a representative, unbiased, population. *i.e.* they represent the steady state distribution of TCOs around Earth. Their sky plane residence time distribution (defined in §A.1) without any constraints on their apparent brightness, distance, rate of motion, *etc.*, shows a strong enhancement near east and west quadrature (see fig. 3.) Their trajectories³ are such that they tend to be furthest from Earth, and therefore moving slowly, at both quadratures so they spend more time there and have the highest sky plane density at that location. The TCOs are strongly enhanced on the ecliptic with the sky plane density dropping off rapidly with ecliptic latitude as for most classes of objects in the solar system as viewed from Earth.

The sky plane number density with constraints on the TCOs’s magnitude and rate of motion shown in fig. 4 is dramatically different from the unconstrained sky plane distribution. Application of the IAU standard H and G_{12} asteroid photometric model (Muinonen *et al.* 2010, we use $G_{12} = 0.5$ throughout this work) eliminates the enhancements at the east and west quadratures observed in fig. 3 in favor of a strong enhancement at opposition due to the photometric surge for very small phase angles. The enhancement along the ecliptic is no longer present because the TCOs must be close to Earth to be detectable which has the effect of increasing their apparent ecliptic latitude distribution. Thus, it is clear that a telescopic optical TCO survey is most effective towards opposition but need not concentrate on the region near the ecliptic. Near-opposition surveying is typically employed by contemporary NEO surveys (*e.g.* Jedicke 1996; Jedicke *et al.* 2002) so we expect that the NEO survey strategy should be finding TCOs or that the next

³We often refer to TCO motion around Earth as a trajectory because their motion often does not follow a nearly-closed elliptical path like the conventional notion of an ‘orbit’.

generation of sky surveys will do so as a matter of course (*e.g.* Tokunaga and Jedicke 2007).

All our results that require calculating the TCOs’ apparent brightness account for Earth’s umbral and penumbral shadowing. Earth’s umbral shadow is about 1° in diameter at 1 LD and is always in the direction of opposition, exactly where the TCO sky plane density is highest. We assume that within the umbral shadow there is zero sunlight and we reduce a TCO’s apparent brightness by $2.5 \log f_\odot$ mag in the penumbra where f_\odot is the fraction of the Sun’s ‘surface’ visible at the TCO. We found that Earth’s shadow makes only a 4% difference in the total sky plane residence time for the detection parameters in fig. 4 and a 5% decrease in the $3^\circ \times 3^\circ$ bin at opposition. The modest shadowing effect even for the relatively bright limiting magnitude is a consequence of requiring that the rate of motion be $< 1^\circ/\text{d}$. The Moon’s rate of motion is about $12^\circ/\text{d}$ so most of the TCOs in the figure must be near or beyond the Moon and mostly unaffected by Earth’s shadow. If an optical survey was capable of detecting faster rates of motion then the Earth shadowing would have a larger effect on the TCO detection capability.

Geocentric TCO apparent rates of motion

In designing a TCO survey strategy (see §3) it is important to understand the TCOs’ rates of motion. Objects that move by more than about 2 PSF-widths during the course of an exposure spread their total flux in a ‘trail’ that reduces the peak S/N in any pixel along the trail compared to stationary objects of the same intrinsic brightness (*e.g.* Vereš *et al.* 2012). Peak pixel detection algorithms are therefore less likely to identify the trailed source. Even algorithms that can identify trailed detections, *e.g.* by summing flux along a line in the image, have reduced sensitivity because the trail’s total S/N is also less than the overall S/N for a stationary object of the same intrinsic brightness. In this work we partly ignore trailing effects because they are detection-system and software-algorithm dependent.

We simply assume that the system will be able to detect objects that are not moving too fast as long as their apparent magnitude is brighter than the system’s limiting value.⁴

TCOs within about 30° of opposition with $V < 20$ and rates of motion $< 15^\circ/\text{d}$ have an average apparent angular speed of about $10^\circ/\text{d}$. (For comparison, the only currently known minimoons, 2006 RH₁₂₀, was discovered about 5° from opposition moving at $\sim 10^\circ/\text{d}$ with $V \sim 19\text{ mag}$). Typical exposure times for contemporary sky surveys are on the order of 60 s so the average TCO would move about $25''$ during the exposure. This could hamper TCO detection by survey systems with small PSFs and pixels because the TCO flux will be distributed over many pixels and create a long trail. Conversely, survey systems with larger PSFs and pixels will be less affected by the TCOs’ motion. Automated trail-identification software or human vetting of TCO candidates could alleviate the loss of detections due to PSF trailing provided that there are not too many image artifacts that mimic trailed detections. Thus, large aperture systems with short exposure and fast readout times would be best for TCO discovery because the large aperture allows the detection of faint objects while the short exposures minimizes trailing losses.

TCO detection at capture in Earth-Moon system

Figure 12 of Granvik *et al.* (2012) provides an idea for how to design a targeted TCO survey (see §3.1). The figure shows that at the moment of capture, the time at which their total energy becomes negative with respect to the Earth-Moon barycenter, most TCOs are 1) in retrograde geocentric orbits 2) near L1 or L2 and just outside Earth’s Hill sphere 3) moving in roughly the same direction 4) at similar rates of motion. Figure 5 shows that

⁴For more information on trail fitting see *e.g.* Vereš *et al.* (2012) who provide a technique for fitting trailed source detections but not how to identify them.

at the time of capture the TCOs are concentrated near the ecliptic in a $\sim 20^\circ$ wide band centered at opposition (the L2 direction). Indeed, there are ~ 6 TCOs larger than 10 cm diameter captured every day in both L1 and L2 (half at each). The objects' motion vectors bring them near the opposition point before or after their moment of capture so that there is a steady stream of small objects in roughly the same direction moving at roughly the same rate of motion. The rates of motion are relatively modest by NEO standards at $1.8 \pm 0.7(\text{rms})^\circ/\text{d}$ with the objects' motion at an average position angle of $274^\circ \pm 38^\circ(\text{rms})$ *e.g.* typically retrograde consistent with most motion along the ecliptic. The trailing rate corresponds to $\sim 0.075''/\text{s}$ so the average TCO trails by about $1''$ in $\sim 13\text{s}$. However, if the telescope is tracked at the mean TCO rate then all the objects with rates within $\pm 1\text{rms}$ of the mean will trail by less than $1''$ in about 34 s. A large telescope with a wide passband filter can reach $V \sim 24.5$ at a good site with $1''$ seeing so that trailing losses can be dramatically reduced for the TCOs in exposures of $\lesssim 60\text{s}$. Furthermore, other TCOs that have already been captured may pass through the same region and contribute more detections to this type of targeted TCO survey. Thus, a targeted deep survey towards the opposition point might detect TCOs near the time of capture and can take advantage of the relatively smooth flow of objects through the region.

Detection of TCOs in the infrared

It may also be possible to detect TCOs in the infrared from space-based platforms or perhaps detections already exist in the WISE spacecraft images (*e.g.* Mainzer *et al.* 2011, §4). If we assume that the TCOs in the size range from 10 cm to 1 m are small enough and/or rotating rapidly enough to be in thermal equilibrium then there is an advantage to detecting the TCOs in the infrared because they are not affected by phase angle effects. The peak of the thermal radiation for a 1 m diameter blackbody object occurs at about

$16\mu\text{m}$ and the peak integrated signal occurs in the $12\mu\text{m}$ W3 passband of the 4 WISE filters (see fig. 6). Thus, the sky plane TCO number distribution in the IR does not have any strong enhancements along the ecliptic as illustrated in fig. 7. Thus, a near-geocentric IR TCO survey (*i.e.* from the ground or relatively low-Earth orbit) would be best served by surveying along the ecliptic as much as possible and then expanding the search to higher latitudes. However, we think a space-based IR survey would be best located at the Earth-Sun L1 Lagrange point from which the majority of TCOs are within a smaller area on the sky in the direction toward Earth (see fig. 7).

Detection of TCO meteors

Finally, we consider detecting TCOs in the final moments of their geocentric trajectory as they enter Earth’s atmosphere (see §3.2 and §5.1) as Granvik *et al.* (2012) showed that about 1% of all TCOs become meteors. These TCO meteors strike the Earth’s atmosphere in a narrow range of speeds with an average of $11.19 \pm 0.03(\text{rms}) \text{ km/s}$ — nearly equal to Earth’s escape speed because the TCOs have essentially fallen to Earth from a large distance with $v_\infty \sim 0 \text{ km/s}$. The impacting TCOs have a flat distribution in $\sin \theta_i$ where θ_i is the impact angle, the acute angle between the TCO’s trajectory and the perpendicular to the Earth’s surface. Thus, the mean impact angle for the TCOs in Granvik *et al.* (2012)’s sample is $44.6^\circ \pm 21.4^\circ(\text{rms})$.

3. Optical Detection

In this section we consider different instances of multiple methods of detecting TCOs in optical light: 1) all-sky, wide area and targeted telescopic surveys and 2) meteor surveys. We make the distinction between all-sky and wide-area because within the next few years

the Asteroid Terrestrial-impact Last Alert System (ATLAS) (Tonry 2011), and possibly the US Department of Defense’s Space Surveillance Telescope (SST), will survey the entire night sky multiple times each night. Other contemporary and anticipated surveys only cover wide areas of the sky each night. The meteor surveys typically either 1) monitor the entire sky visible from their locations each night but necessarily to a relatively bright limiting magnitude (*e.g.* Spurný *et al.* 2007) or 2) perform a deeper survey over narrower fields, often using image intensified video systems (Hawkes 2002; Weryk *et al.* 2013). A meteoroid orbit survey described in Jenniskens *et al.* (2011) accomplishes both goals using a ‘fly’s eye’ approach with low-light video cameras and multi-station imaging.

Optical surveys with limited coverage should target the region near opposition since TCOs are enhanced in the optical in the anti-Sun direction (see fig. 4), and expand their TCO search outwards from opposition as the survey permits. Surveys with fainter limiting magnitudes will have higher TCO discovery rates and those with software capable of identifying the trailed TCO detections will also have an advantage over those surveys that can only identify detections with stellar PSFs.

3.1. Telescopic Detection

We considered in detail four different instances of optical telescopic surveys with which we have some familiarity and focussed on next-generation surveys with wide field coverage or a targeted survey to a faint limiting magnitude with a next-generation camera (see table 1).

Catalina Sky Survey (CSS)

The only known TCO, 2006 RH₁₂₀, was discovered during routine survey operations by the Catalina Sky Survey (CSS, Larson *et al.* 1998; Kwiatkowski *et al.* 2009) so that survey’s TCO detection capabilities have already been demonstrated. The CSS has operated 2 or 3 telescopes in the northern and southern hemispheres for about a decade and is currently the leading NEO discovery survey. Their two northern hemisphere telescopes (observatory codes G96 and 703) serve the complementary purposes of a relatively deep and narrow survey along with a shallow and wide survey. Each of their sites currently delivers roughly comparable numbers of NEO discoveries to the Pan-STARRS1 system described in more detail below (almost identical for G96 and within about 50% for 703).

Panoramic Survey Telescope and Rapid Response System (Pan-STARRS1)

The Pan-STARRS1 survey has been in operation since the spring of 2010. The 1.8 m telescope with an $\sim 7 \text{ deg}^2$ field of view discovers most of its moving objects in 45 s exposures obtained with their wide-band w_{P1} filter. Since the onset of operations they have surveyed about $7,700 \text{ deg}^2/\text{month}$ in modes suitable for TCO detection to a limiting magnitude of $V \sim 21.7$. Pan-STARRS1 has not yet implemented trail detection and currently has essentially zero efficiency for identifying objects moving faster than about $3^\circ/\text{d}$ (Denneau *et al.* 2013).

Since we have more experience with the Pan-STARRS1 system we will use it’s *current* performance characteristics to model TCO detections but the results will also be roughly representative of the CSS G96 site (roughly similar limiting magnitudes and nightly survey area). Our choice of system characteristics is motivated by our desire to ensure that 1) we use realistic NEO survey detection characteristics of an existing survey and 2) our estimates

represent a lower limit to the TCO detection capabilities of the more capable and upcoming NEO surveys.

In its current mode of operations Pan-STARRS1 should detect about 10^{-2} TCOs/lunation so it is unsurprising that it has not yet reported a TCO discovery. However, it is likely that they have already imaged trailed TCOs that were not identified by their image processing pipeline or linked by the moving object processing system — a large great circle residual (GCR⁵) of the detections within a tracklet relative to the astrometric uncertainty makes it difficult to link the detections into tracklets. Furthermore, even if a TCO was detected and reported to the MPC it is unlikely that it could be reacquired by followup observatories because of the relatively large ephemeris uncertainty, which is due to their high rates of motion, and the fact that Pan-STARRS1 typically requires 8-12 h to report moving objects.

We expect that these problems will be dramatically reduced over the next few years as Pan-STARRS1 and CSS are upgraded and other NEO surveys come online. The implementation of trail-identification software and decreasing the time delay between image acquisition and reporting candidate discoveries to the MPC will increase the likelihood of TCO discoveries. Starting in April 2014 the Pan-STARRS1 system was dedicated 100% of the time to NEO surveying and it will be joined by a second telescope, Pan-STARRS2, within the next two years (Wainscoat *et al.* 2013). At the same time, the CSS G96 system will increase the area of its field of view by a factor of ~ 4 , while the CSS 703 site will increase the area of its field of view by a factor of ~ 2.4 (Christensen *et al.* 2012).

⁵the astrometric RMS of the detections relative to the best-fit great circle

Asteroid Terrestrial-impact Last Alert System (ATLAS)

The ATLAS survey is expected to begin regular operations in early 2016 (Tonry 2011). They plan to survey the entire sky $4\times$ each night to $V \sim 20$ with relatively small but very wide-field telescopes. The system has one major limitation from the perspective of detecting TCOs — its relatively bright limiting magnitude — but this is compensated somewhat by its $\sim 4''$ pixels that dramatically reduce trailing losses. The large pixel scale and associated large astrometric uncertainties limits their ability to detect all but the largest GCRs (see fig. 8) but they expect to deliver moving objects to the MPC within minutes of the final image acquired at a boresite so that followup activity can begin almost immediately. There are about 8.4×10^{-3} TCOs at any time on the night sky with $V < 20.0$ and $\omega < 15^\circ/\text{d}$, a rate of motion that will leave just 5 pixel long trails on the ATLAS images. We thus expect that ATLAS should detect about 0.1 TCOs/lunation or, equivalently, about a 85% chance of detecting a TCO in its first year of operation. One advantage to the bright limiting magnitude is that almost all moving objects with $V < 20$ will already exist in the MPC catalog so that any new moving object that appears in the ATLAS survey must be interesting — *e.g.* an NEO, asteroid cratering or disruption event, or TCO. While the ATLAS TCO detection rate might be relatively low it is guaranteed that the discovered objects will be bright, large, and relatively easy to track over many nights.

Space Surveillance Telescope (SST)

We include in table 1 a row for the DoD’s Space Surveillance Telescope (SST; *e.g.* Monet *et al.* 2013) because it will almost certainly become the leading asteroid discovery survey if it is directed to search for NEOs and performs as expected. It is currently tasked with surveying the sky close to the equator for artificial satellites but may eventually incorporate a sizable NEO survey component much like the history of the Lincoln

Near-Earth Asteroid Research system (LINEAR; *e.g.* Stokes *et al.* 2000). The SST’s short exposures limit TCO trailing losses and their all-sky coverage to $V \sim 22$ make ~ 0.4 TCOs available to the system on the sky plane at any time. Like ATLAS, SST surveys the entire sky every night so it is natural that there are $\sim 50\times$ more TCOs available to SST on the sky but because it surveys ~ 2 magnitudes fainter than ATLAS it ‘saturates’ on the TCOs, *i.e.* finds the available ones, and the sky takes longer to ‘refresh’ so that the TCO discovery rate per day is only about double the ATLAS rate.

Large Synoptic Survey Telescope (LSST)

The Large Synoptic Survey Telescope (LSST) is nearly the ultimate TCO detection machine with its $\sim 9.6 \text{ deg}^2$ FOV, $V \sim 24.7$ limiting magnitude, and 15 s exposure pairs, but it ‘only’ surveys about 20-25% of the sky each night (Ivezic *et al.* 2008). Its short and back-to-back pairs of exposures should make identifying fast moving objects easy and eliminate much of the confusion from systematics and noise in the image plane. Their $0.2''$ pixel scale in combination with their excellent site on Cerro Pachón will mean that most TCO detections will be trailed in their 35 s exposures (a 15 s back-to-back exposure pair with an intervening 5 s read out time). Our LSST TCO detection estimate in table 1 used a peak rate of detectable motion of $10^\circ/\text{d}$ for which a TCO would leave a 33 pixel long trail in the system’s focal plane. We expect that LSST could detect about 1.5 TCOs/lunation but a major problem with this success rate is that most will be too faint for followup by other observatories. Another possible problem is that with only 2 detections/night it will be difficult to measure the GCR. Two possible ways to ameliorate the problem are to 1) treat the 2 exposures in a back-to-back pair as two separate detections which would provide 4 detections per night or 2) it may be possible that the trails in the two exposures have slightly different position angles due to parallax. The additional spatial information from

the parallax would allow for a significant reduction in the ephemeris uncertainty. By the time LSST re-images the same TCO, if it is still visible at all, the object will have moved a considerable distance on the sky and manifest itself with an entirely different rate of motion, position angle, and apparent brightness.

Subaru telescope with Hyper Suprime-Cam (HSC)

A targeted survey with Hyper Suprime-Cam (HSC; Takada 2010) on the Subaru telescope located on Mauna Kea, Hawaii, could be very effective at discovering TCOs. The 870 Mpix HSC with a $\sim 1.5^\circ$ wide FOV mounted on a 8.2m telescope at one of the best sites in the world could detect small TCOs when they are well beyond the Moon. For our study we assumed that the HSC can reach $V = 24.5$ for point sources in 15 s exposures with sidereal tracking.⁶ We restrict our calculation to those TCOs with apparent rates of motion $< 1^\circ/\text{d}$ so as to limit the effects of trailing of the detections to less than a typical PSF of $\sim 0.6''$. With a 20 s readout time this system could survey $\sim 450 \text{ deg}^2/\text{night}$ centered on opposition and allow detection of TCOs of only 0.5 m in diameter at their mean geocentric distance of $\sim 4.0 \text{ LD}$. While there are ~ 1.1 TCOs visible in the night sky with $V < 24.5$ and moving slower than $1^\circ/\text{d}$ the targeted HSC survey should detect about 0.4 TCOs/night in the survey area or, equivalently, have a $\sim 90\%$ chance of detecting a TCO in a 5-night observing run spread over 40 days (because the TCO refresh time is about 8 d - see table 1).

⁶Our assumption is based on the Subaru SuprimeCam exposure time calculator (http://www.naoj.org/cgi-bin/img_etc.cgi) for the r' filter but is somewhat more optimistic because we assume that a minimoon survey would either use no filter or a wide-band filter.

Identifying TCOs by their great circle residual (GCR)

Large GCR’s relative to the astrometric uncertainty can provide better short-arc ephemerides for the TCOs. Figure 8 shows that GCRs for the 4 different optical surveys decrease with increasing geocentric distance as expected. A ‘plume’ of TCOs with GCRs $\gg 1''$ is due to the rare TCOs that are very close to Earth but still moving slow enough to be detected by the survey. For the ATLAS survey the GCR is typically much less than the astrometric uncertainty so that TCOs must be distinguished by their fast rate of motion rather than GCR. Most of the TCOs that can be detected by the wide-field cameras with small pixel scales will have significant GCRs that should help in identifying them (assuming the detections can be linked into tracklets) and also in calculating their ephemerides for subsequent followup. The lower-left panel in fig. 8 shows that most TCOs will not be detectable with measurable GCR by LSST. Our simulation assumed that LSST would obtain 2 back-to-back exposures with 5s time difference and 60 min later obtain another back-to-back set. We have further assumed that the detections from each of the 4 exposures will be identified rather than identifying only 2 detections in the stacked back-to-back pairs. While this cadence has many advantages to the image processing pipeline it is not conducive to identifying TCOs.

Detectable TCO diameters

The surveys discussed above are sensitive to TCOs from a few cm to tens of cm diameter and the size of the object at the peak in the number distribution decreases with the aperture of the survey telescope (see fig. 9). The ATLAS survey has a peak sensitivity to TCOs with $H \sim 31$ or about 2m in diameter. The problem is that there are only 1-2 objects of this diameter in orbit at any time and the probability that they pass near opposition is relatively small (where the phase angle is close to zero at a close enough

distance to be detected by ATLAS). Pan-STARRS1 could do much better than ATLAS but is limited by the relatively small amount of time devoted to surveying for moving objects and its inability to identify trails in the images. The wide area LSST and targeted HSC surveys both have good sensitivity to TCOs of sub-meter diameter. The HSC survey discovers slightly larger TCOs than the LSST even though they have roughly the same limiting magnitude because we have restricted the maximum rate of motion to $< 1^\circ/\text{d}$, which means that the TCOs must be more distant and therefore larger to be detectable. This advantage makes the TCOs easier to detect in dedicated followup efforts with *e.g.* radar or other optical telescopes.

3.2. Meteor Survey Detection

The Granvik *et al.* (2012) NEO capture simulation yielded 18,096 TCOs of which 189 or $\sim 1\%$ eventually struck Earth. They normalize their results to the Brown *et al.* (2002) bolide data and argue that about 0.1% of meteors are TCOs prior to striking the atmosphere.

Considering that all-sky meteor surveys have existed for decades, and that modern networks like ASGARD (southern Ontario, Canada, Brown *et al.* 2010), CAMO (Elginfield, Ontario, Weryk *et al.* 2013), and CAMS (California, USA, Jenniskens *et al.* 2011), have the capability of measuring the pre-meteor phase orbit, it might seem surprising that there are no reports that 1 in a 1,000 meteors were originally in geocentric orbit. The solution to the puzzle is that not all meteors are equally visible. The apparent brightness of a meteor $\propto m^{-2.02 \pm 0.15} s^{-7.17 \pm 0.41}$ where m is the meteoroid’s mass and s is its speed and we ignore an insignificant dependence on the zenith angle that is consistent with zero (Sarma and Jones 1985; Campbell *et al.* 2000). Thus, a meteor’s apparent brightness is exceedingly sensitive to its speed in the atmosphere.

Detecting TCO meteors with Cameras for Allsky Meteor Surveillance (CAMS)

Meteoroids must have a mass $\gtrsim 0.6$ g to be detected by CAMS at the TCOs’ sluggish ~ 11.2 km/s geocentric impact speed if we use a limiting V magnitude of +3.0 (Jenniskens *et al.* 2011). This suggests that TCOs must have a diameter of more than about 8 mm to be detected assuming a typical meteorite grain density of 3.0 g/cm³ (Britt and Consolmagno 2004).

We calculate that from Oct 2010 through December 2011 CAMS observed about 1.7 meteors/year with geocentric impact speeds consistent with being in the TCO speed range of $[11.16, 11.22]$ km/s. The calculated rate is the cumulative probability density of all detected meteors with reported speeds within 3σ of the central value of 11.19 km/s. Extrapolating from the Brown *et al.* (2002) meteoroid SFD down to 8 mm diameter suggests that there are $(21 \pm 2) \times 10^3$ TCOs of this size or larger striking Earth every year corresponding to about $(4.1 \pm 0.4) \times 10^{-5}$ TCOs/km²/year. The CAMS system monitors the sky above an altitude of about 30° and at a typical meteor phase onset altitude of about 75 km the system therefore monitors about 3×10^4 km². Accounting for the fact that the survey can only operate at night (about 10 h/d) and for 30% weather losses we estimate that CAMs should detect about 0.4 TCO meteors/year.

The agreement to within a factor of about 4 between the predicted and observed rate of meteors with TCO-like speeds is incredibly good considering all the unknowns and uncertainties. However, the agreement should not be over interpreted, any value within a couple orders of magnitude could have been argued as being due to detection efficiency within the CAMS system, errors in the TCO model at the smallest sizes due to Yarkovsky, contamination of the CAMS TCO-like speeds by underestimated uncertainties or artificial satellite debris, *etc.*

Detecting TCO meteors with the All Sky and Guided Automatic Realtime Detection system (ASGARD) and the Canadian Automated Meteor Observatory (CAMO)

The ASGARD all-sky system has been in operation for about six years and recently detected its first TCO-like meteor with an atmospheric entry speed of 11.2 ± 0.8 km/s and mass of ~ 100 g (about 44 mm diameter). Its speed is consistent with that expected for TCO meteors but there is only a 10% probability that it is actually a TCO-like speed if we assume a Gaussian distribution in the speed uncertainty.

We estimate that ASGARD, with a limiting sensitivity of $V \sim -2$, should see about 0.01 TCOs/year of this size or larger implying that its detection of a TCO-like meteor in only six years would be unusual — perhaps $\sim 15\times$ higher than what we predict from the TCO model. On the other hand, with only a 10% chance that the ASGARD object has a TCO-like speed perhaps the numbers are in excellent agreement. Once again, we do not want to speculate too much on a disagreement between the predicted and observed TCO meteor rate for the same reasons as discussed above for CAMS.

Finally, the narrow-field influx cameras which are part of the CAMO system have been in two-station operation for 3 years. In that time a total of 685 h of observation have been manually reduced resulting in 5,047 high quality double-station meteors. An upper limit to the system’s collecting area at heights corresponding to an ablation altitude appropriate to a 12 km/s entry speed (90 km) is ~ 350 km². At TCO geocentric impact speeds of ~ 11.2 km/s the limiting sensitivity of this system is $V \sim +6$ corresponding to meteoroids with masses of ~ 0.01 g. We identified 8 candidate TCO events with derived masses between 0.01-0.12 g (average ~ 0.04 g) using the luminous efficiency from Ceplecha and McCrosky (1976) after detailed examination of all 5,047 meteors, eliminating those with poor geometry (Musci *et al.* 2012), and retaining only those with speeds (based on the average speed during the first half of their visible trails) within 1σ of 11.2 km/s . Manual

examination of the solutions for the 8 events shows that 3 have convincing dynamic flight solutions with geocentric impact speeds at or below 11.2 km/s. The other five events show varying degrees of deceleration more suggestive of true initial speeds above 12 km/s.

It is clear that it is difficult to determine accurate masses and speeds of the meteors in the range of detectable TCOs but, for comparison, a 0.04 g meteoroid has $H \sim 45.5$. We predict that there are about 650 TCO meteors per day over the Earth’s entire surface with $H < 45.5$ and that CAMO should have seen about 0.01 of them given its observing time, sky coverage, weather losses, dark time, *etc.*. The two orders of magnitude discrepancy between our prediction for the number of TCO meteors that CAMO detects and their actual results are in stark contrast to the factor of 4 under prediction for CAMS (see above). We attribute the differences to the difficulties in measuring meteor speeds, and especially their masses, coupled with our extrapolation of the TCO SFD to meteoroids that are almost ten orders of magnitude smaller in mass than those that anchored the Granvik *et al.* (2012) TCO SFD.

4. Space-based Infrared Detection of TCOs

Ground-based infrared facilities do not currently have the sensitivity and wide-fields necessary for the TCO survey but the successful WISE spacecraft mission (*e.g.* Wright *et al.* 2010) and its asteroid-detecting NEOWISE sub-component (*e.g.* Mainzer *et al.* 2011) shows that space-based IR surveys can be very effective (see fig. 7). (Our method of calculating the IR flux from TCOs is outlined in A.4.) Thus, we use the NEOWISE mission as a baseline for an IR TCO survey even though future IR spacecraft surveys such as the proposed NEOCam mission (McMurtry *et al.* 2013; Mainzer 2006) will certainly be even more effective at asteroid discovery.

To characterize the utility of a space-based TCO survey we estimate the number of TCOs that might have been detected by NEOWISE in their cryogenic $12\mu\text{m}$ W3 band images, the band most sensitive to meter-scale TCOs as described in §2. Images in this band were sensitive to sources with flux $\Phi_{W3} > 0.65 \text{ mJy}$ (Wright *et al.* 2010) and the fastest solar system object they reported to the MPC was moving at $3.22^\circ/\text{d}$. The WISE FOV was $47'$ with a 90 minute re-visit time at each sky location. In the worst-case scenario a TCO moving at up to $6^\circ/\text{d}$ should still be detected $3\times$ but in practice NEOWISE required that the object be detected $> 3\times$ to reduce the false detection rate. We find that there are ~ 1 TCOs on the entire sky plane brighter than the specified flux limit and moving slower than a slightly more conservative $3^\circ/\text{d}$ (see fig. 7). This corresponds to about 0.005 TCOs in a $47'$ wide strip extending 360° around the sky through the east and west quadratures — the region surveyed by WISE in a 90 minute time interval. With a ~ 2 day refresh time for TCOs with these properties we calculate that WISE had about a 7% probability of detecting one in each of the 10 months of the survey or about a 50% chance of detecting one TCO during the spacecraft’s W3 band’s operational lifetime.

WISE’s peak sensitivity is for TCOs in the 1 m size range — well-tuned to the expected size of the largest TCOs expected in the steady-state (see fig. 9). Since the WISE mission’s cryogenic lifetime of about 10 months is well matched to the average TCO lifetime it is likely that a WISE-like survey would detect one of the 1-2 one-meter scale TCOs in orbit around Earth at any time. Larger objects are unlikely to be detected simply because they are unlikely to be captured and the smaller objects are not detected due to the flux limitations. Thus, a NEOWISE-like spacecraft mission could be an effective technique for detecting the largest, and therefore most interesting, TCOs available in the steady state.

NEOWISE is not known to have reported a TCO to the MPC despite our calculation that it had a $\sim 50\%$ TCO detection efficiency. There are several possible explanations for the

lack of a TCO detection including, in no particular order of likelihood: 1) the probability of NEOWISE *not* detecting a TCO was also 50% 2) TCOs will have higher GCRs than the NEOs that NEOWISE was tuned to detect and may therefore not be detected with the same efficiency 3) ground-based followup of NEOWISE’s NEO candidates was required to confirm their NEO status, but ground-based followup sites assume that the objects are on heliocentric orbits when creating ephemeris predictions so that recovery of objects that are actually on geocentric orbits will be unlikely if not effectively impossible and, finally, 4) it is always possible that our TCO model is incorrect.

WISE was not originally designed to identify asteroids and was not optimized for TCO discovery. This work concentrates on the capabilities of existing assets in detecting TCOs but we have begun studies to examine the capability of IR spacecraft optimized for TCO discovery. Our first tests assumed that 1) the spacecraft will be located at the Sun-Earth L1 point so that the highest TCO sky plane density and Earth are at opposition as viewed from the spacecraft (the sky plane distribution is illustrated in fig. 7) 2) mirror diameters of 0.25 m, 0.5 m and 1 m and 3) the use of the WISE W3 passband with sensitivity from about $7.5\,\mu\text{m}$ to $16\,\mu\text{m}$ as illustrated in fig. 6. Under these assumptions our calculations suggest that there are about 1, 5 and 30 TCOs respectively on the sky plane *at any time* which suggests that this type of mission could provide a steady stream of TCOs for ground-based physical characterization (rotation state, colors and/or spectra) or even opportunities for rendezvous, retrieval, or resource studies and utilization (*e.g.* Chyba *et al.* 2014). Actual TCO surveys in the IR from L1 would need to avoid surveying too near the Earth and Moon but detailed modeling of their performance is beyond the scope of this work even though the prospect of TCO discovery with this type of mission is promising.

5. Radar Detection

There are multiple radar systems capable of detecting TCOs either while in orbit around Earth or as they plummet through the atmosphere.

There is little in the literature about detecting meteoroids but a 1994 DoD space surveillance network campaign (Schwan 1995) identified 3 objects on similar orbits whose large semi-major axes, high eccentricity and retrograde inclinations were surprising at the time because the ‘origin of satellites in this region is uncertain’. The 10 to 20 cm diameter objects (larger if they were actually stony asteroids) did not correspond to any known launch and the study concluded that this ‘class of debris object may warrant further evaluation’. Their orbits matched the TCO orbit distribution very well. There is no doubt that the capabilities of the Air Force Space Surveillance Systems have improved in the past twenty years and they may now be capable of regularly discovering TCOs.

In the remainder of this section we focus on detecting TCOs with existing mono-static and bi-static radar facilities (*e.g.* Arecibo and Green Bank) and meteor radar facilities that are available to the scientific community.

5.1. Meteor Radar Detection

Ground-based meteor radar systems efficiently detect the ionization left behind in the atmosphere as a meteoroid ablates. They typically have high power and large aperture (HPLA) because the radial scattering cross section is small. The radar echo is often referred to as ‘head’ echoes (Baggaley 2002).

The radar detectability of meteors has been found empirically to be $\propto m^{0.92}s^{3.91}$ (Verniani 1973) where m is the mass of the meteor in grams and s is the speed in km/s, but the dependence on speed becomes much steeper at the small speeds typical of TCO

meteors (Weryk and Brown 2013). Our examination of ~ 4 million speed estimates made by the Canadian Meteor Orbit Radar system (CMOR; Jones *et al.* 2005) found 1,790 with speeds below 11.2 km/s. Without additional information it is not possible to determine if any were TCOs as opposed to a decelerated, unbound meteoroid, as all of these detections were below 85 km altitude where the meteors have already decelerated due to atmospheric interactions at higher altitudes.

TCO head echo detection with HPLA is difficult because the small HPLA beam size corresponds to a limited atmospheric collecting area of order a few to 10s of km^2 or less (*e.g.* Brown *et al.* 2001; Murray *et al.* 2004) but they have the capability of detecting ablation masses larger than about 10^{-8} kg (Ceplecha *et al.* 1998). Measured HPLA meteoroid speed distributions show a strong peak at ~ 55 km/s with only a few detections at TCO impact speeds of ~ 11.2 km/s (Hunt *et al.* 2004). Our predicted HPLA TCO detection rate is about 8/year after extrapolating down to these tiny masses with the nominal Granvik *et al.* (2012) model. *i.e.* the HPLA systems should detect about 8 TCO meteors/year if they are 100% efficient and operating 24 h/d and 365 d/yr. The factor of 2-3 \times difference between the predicted TCO rate and the observed HPLA rate is not significant given the uncertainty in the extrapolation to the small TCO sizes and the reality that HPLA systems are not 100% efficient all the time.

5.2. Direct meteoroid radar detection

There have been long-standing efforts to detect orbital debris with radar (Stokely *et al.* 2009) but the only reported attempt to directly discover meteoroids in space with radar was with the NORAD PARCS system (Kessler *et al.* 1980). They identified 31 candidates in 8.4 hours of observations with an average diameter of ~ 7 cm ($H \sim 39$), comparable to the size of the TCOs in this study. However, these meteoroids were not gravitationally bound to

Earth because their geocentric speeds were significantly higher than Earth’s escape speed *i.e.* they were not TCOs.

Detecting known asteroids by their reflected radar signals is now routine at the Arecibo and Goldstone facilities where over 450 Near Earth Asteroids (NEA) have been detected.⁷ They bounce radar off asteroids on a weekly basis and the smallest detected objects to date are⁸ 2012 XB₁₁₂ and 2006 RH₁₂₀ (the latter being the only known TCO), both with $H \sim 30$ corresponding to 2-3 m in diameter. However, they have not discovered new asteroids other than the orbiting companions of the targeted objects because the radar beam has limited angular coverage and sensitivity that drops off like Δ^4 where Δ is the geocentric distance.

Figure 10 shows that the TCO’s range and range-rate distributions are within Arecibo’s mono-static radar detection capabilities (in which the site both transmits and receives the radar signal). A 100 cm/25 cm diameter non-rotating TCO is detectable if it is within $\sim 11 LD / \sim 6 LD$ (we assume a minimum $S/N=2.3$ per second of integration time as described in more detail below). The problem is that the reflected signal is doppler spread by the object’s rotation and at some size- and range-dependent rotation rate the received S/N will be below the system’s detection limit.

The rotation rate distribution of meter-scale meteoroids is addressed in §A.6 where we describe our technique for estimating the spin-rate distribution for TCOs of less than 10 m diameter. While the predicted median spin rates for objects of the size we expect to identify with radar render them undetectable by current radar assets there is a long tail of slow-rotating meteoroids that can be detected.

Our calculations (see §A.5 for an overview of calculating radar detectability of

⁷as of May 2014 — <http://echo.jpl.nasa.gov/asteroids/>

⁸<http://echo.jpl.nasa.gov/~lance/small.neas.html>

asteroids) suggest that detecting TCOs is essentially impossible with mono-static operations at Arecibo because their minimum detectable geocentric distance of 4-5 LD is fixed by the time to switch between transmitting and receiving and there are simply not enough TCOs rotating slow enough beyond that distance to make the technique viable (see fig. 10). The Goldstone array has the capability of observing objects as close as 2 LD, but the increase in signal from the decrease in the minimum observable distance is not enough to overcome the several factors decrease in sensitivity compared to the Arecibo array.

Detecting TCOs with bi-static radar

There may be opportunities to discover TCOs using bi-static operations where the radar signal is transmitted by Arecibo and received at Green Bank (Benner *et al.* 2002). Routine radar detection of known asteroids requires that the object’s topocentric range and range-rate be known so that the returned signal is sampled in the appropriate range and range-rate bins. A search for unknown TCOs requires identifying the reflected signal in range-rate phase space (see fig. 10) and to do so requires limiting the range-rate extent and binning the returned signal.

For our simulations we restrict the search to $-1 \text{ km/s} < \dot{\Delta} < +1 \text{ km/s}$ because $\sim 96\%$ of the detectable TCOs are found within this range. The range-rate dimension was binned by 10 cm/s because $> 99\%$ of all TCOs have accelerations of $< 10 \text{ cm}^2/\text{s}$ (*i.e.* not just the detectable ones; see fig. 11) and we will assume 1 s integration times so that a TCO remains in one bin during each transmission. Our simulation also assumes that each telescope pointing direction will be scanned with up to 12 one-second transmissions. At the maximum allowed acceleration the TCO’s range-rate may be in a different bin in each scan, reducing the S/N in an individual scan by a factor of about $3.5 \sim \sqrt{12}$. Our experience with radar asteroid detection suggests that the minimum S/N is ~ 2.3 so that

we require the total received $S/N=8$ for a TCO detection. We used a realistic transmitting power of 0.9 MW and a conservative radar albedo of 0.15 typical for S-type NEOs⁹ and calculated the returned S/N accounting for the TCO’s rotation rate as described in A.5. Each radar pointing direction has an $\sim 2'$ beam width in which we calculate there are $\sim 4 \times 10^{-6}$ detectable TCOs at any time at opposition and $\sim 3 \times 10^{-5}$ at the quadratures. These values correspond to about 5×10^{-3} and 3×10^{-2} detectable TCOs/deg² at the two locations respectively.

The detectable TCOs are dominated by objects with $\Delta \lesssim 0.5$ LD and $-1 \text{ km/s} < \dot{\Delta} < +1 \text{ km/s}$ (fig. 10) and must be objects in the tail of the rotation period distribution with long rotation periods (on the order of minutes or more). Since the objects are so close to Earth their apparent transverse speeds are high and the refresh rate of objects in the radar beam is about 10 min towards opposition and 30 min towards the east and west quadratures. However, since the TCO residence time is enhanced towards the east and west quadratures at distances less than 1 LD (fig. 1), the probability of discovering a TCO towards the east and west quadratures is larger than towards opposition. The east or the west quadrature is always observable by Arecibo for at least 7-8 hours every day despite the pointing limitations of the array.

Arecibo has a 20% probability of detecting a TCO in 40 h of observing in the east and/or west quadratures when we use our conservative assumptions about the TCO rotation rate distribution as described in §A.6. However, we have empirical evidence that suggests the rotation rate distribution is non-Maxwellian since it does not provide a good fit to rotation rates of small asteroids in the Light Curve Database (LCDB, Warner *et al.* 2009). The actual rotation rate distribution suggests that $\sim 10\%$ of asteroids with

⁹The average of many published values summarized at http://echo.jpl.nasa.gov/~lance/asteroid_radar_properties/nea.radaralbedo.html.

$H > 25$ have rotation rates that are slow enough to have a negligible effect on their radar detectability at geocentric ranges within a few LD. The probability of detecting a TCO with 40 h of observing time increases to 30%, 60% and 80% if we assume that 1%, 5% and 10% of TCOs respectively are rotating slow enough to be detectable as suggested by the LCDB data (fig. 12). (All our radar results impose a lower diameter limit of 3 cm because Rayleigh scattering starts to have a significant effect on the detection of objects of about 3 cm diameter because the radar wavelength is 13.6 cm (Knott *et al.* 2004).)

Our results suggest that radar-detected TCOs have a very different orbit distribution from the entire steady-state population. Fully 85% of the radar-detected TCOs at the quadratures have TCO lifetimes of $> 2,000$ d compared to just $\sim 0.3\%$ of the entire steady-state population (Granvik *et al.* 2012). The orbital element distribution of all radar-detectable TCOs compared to the orbital element distribution for radar-detectable TCOs with lifetimes in excess of 2,000 d tend to have smaller semimajor axes (fig. 13). The preferential detection of the long-lived TCOs has implications for spacecraft TCO rendezvous missions because they have the advantage of being accessible by spacecraft for years after their discovery (Chyba *et al.* 2014).

6. Discussion

We have shown above that it will be challenging but not impossible to discover TCOs on a regular basis with existing facilities but the scientific and exploration opportunities might generate enough interest to dedicate resources to the task.

One TCO discovery opportunity that was not explored above is data mining of the Minor Planet Center’s (MPC) so called one-night-stand (ONS) file. This list of detections that have never been linked to known heliocentric objects with longer arcs could be searched

specifically for geocentric objects. As mentioned in the introduction, we have anecdotal evidence suggesting that unknown geocentric objects were/are discovered and followed by asteroid surveys but they are not flagged as interesting by the MPC because it is difficult or impossible for them to distinguish these objects from operational spacecraft or space junk. However, the work of Granvik *et al.* (2012) provides a means of comparing the derived geocentric orbit to those expected for TCOs which are typically very different from artificial satellite orbits. Given the short arc lengths and lack of spectroscopic or even colors of these historical ONS detections it is unlikely that any TCO could ever be confirmed, but if there were enough detected objects it might be possible to compare the distribution of their geocentric orbits with the expected TCO distribution.

Of course, there will always remain the possibility that the detected objects were classified satellites because the types of orbits occupied by TCOs are also the types of orbits that might be desirable for ‘hiding’ spacecraft — objects on these orbits would spend a significant fraction of their time far from Earth where they are very faint, and when they are brighter and closer to Earth they would be moving extremely fast. Either way, the objects are difficult to detect.

This work has addressed only the issue of TCO discoverability and ignored issues related to observation cadence, followup, and time of discovery relative to time of capture — all important issues for determining the viability of observation programs that would target the TCO for physical characterization or spacecraft missions that might attempt to intercept or even retrieve the object (Chyba *et al.* 2014). This kind of work would require a high fidelity simulation of an asteroid survey system capable of integrating the TCOs within the Earth-Moon system.

Even if TCOs are discovered by operational surveys it is important to understand whether their orbits can be determined quickly and well enough to allow followup or a

spacecraft mission. As is well known from NEO followup efforts, short-arc extrapolation of discovery tracklets for ‘simple’ heliocentric NEO motion can quickly lead to ephemeris sky plane uncertainties of many deg^2 making recovery impossible. We have begun to study the evolution of the orbital uncertainties and error as a function of a TCO’s observational arc and find that the TCOs’ orbits converge rapidly due to their proximity and the advantage afforded the orbit determination by their topocentric parallax (Granvik *et al.* 2013). It is our expectation that just a dozen TCO observations over a few days should allow the orbit to be known well enough to enable radar detections which will then dramatically refine the orbit.

TCOs discovered with optical and radar assets may be distinguished from space debris by their geocentric orbital elements. The vast majority of space debris have circular geocentric orbits within 300 km (8×10^{-4} LD) of the Earth’s surface (Tingay *et al.* 2013) where as TCOs which come within such a close distance have highly eccentric orbits (fig. 13). This comparison could rule out artificial from natural satellites as soon as the orbital solutions of a TCO candidate were determined.

TCOs may also be distinguished from space debris by their bulk density that could be measured by examining how a candidate TCO is affected by radiation pressure (*e.g.* Micheli *et al.* 2013). Indeed, the trajectory of 2006 RH₁₂₀ could not be reproduced without accounting for the effects of radiation pressure acting on the few-meter diameter object. Precision ephemeris measurements with ground-based optical telescopes over the course of days or weeks could measure the radiation pressure on the small TCOs (personal communication with Marco Micheli, 2013), or sooner with repeated radar observations given their superior range and range-rate determination. We expect that TCOs will have bulk densities similar to porous rock (1 g/cm^{-3} ; Britt and Consolmagno 2004) but artificial objects on the meter-scale will have much smaller values *e.g.* the Apollo 12 fourth stage

was recaptured in the Earth-Moon system on a TCO-like orbit but its bulk density was $\sim 0.02 \text{ g/cm}^{-3}$

Finally, compositional information obtained with radar or spectroscopic follow up observations could be used to rule out or determine artificiality of TCO candidates. Such was the case with the object designated as J002E3 that was conclusively linked with the Apollo 12 fourth stage¹⁰.

7. Conclusions

The detection of Earth’s temporarily captured orbiting (TCO) asteroids is challenging due to the small number of objects in the population in the steady state, their small sizes (the largest being only on the order of 1 to 2 m diameter), their large geocentric semi-major axes, and highly eccentric orbits. Despite these challenges we find that a space-based IR survey system could be effective at discovering the TCOs. There may be up to a few dozen TCOs detectable on the sky plane at any time in the IR with a moderate size mirror (0.5 to 1.0 m) on a spacecraft located near the Earth-Sun L1 point (§4). This kind of survey system might be justified from the standpoint of identifying objects that could be stepping stones to learning how to exploit near-Earth natural resources *e.g.* developing techniques for navigation, interaction with, and mining small asteroids. A targeted ground-based TCO survey with a wide-field camera on a large telescope could be effective for testing the Granvik *et al.* (2012) model *e.g.* our calculations suggest that a TCO survey with Hyper Suprime-Cam on the Subaru telescope (§3.1) has about a 90% chance of detecting a TCO in a dedicated 5-night survey. While this survey is useful for testing the principle it would not be an effective means of guaranteeing a steady stream of TCOs for scientific

¹⁰http://www.jpl.nasa.gov/releases/2002/release_2002_178.cfm

followup or rendezvous and retrieval missions. Finally, it is possible that TCOs may be directly discoverable with bi-static radar (§5.2) but this possibility relies on the rotation rate distribution being strongly non-Maxwellian for the small TCOs. The long-lived TCOs discovered in this way would be valuable targets for small asteroid characterization and rendezvous or retrieval missions.

Acknowledgments

This work was supported in part by NASA NEOO grant NNX08AR22G. PGB acknowledges funding support from co-operative agreement NNX11AB76A and the Canadian Natural Sciences and Engineering Research Council. MG was funded by grant #137853 from the Academy of Finland. MCN and ESH were supported under NEOO grant NNX12AF24G.

A. Appendix

A.1. Sky plane residence time distribution

We define the sky plane residence time T_j for a particle j as the time it spends near ecliptic longitude λ and latitude β in the intervals $[\lambda - \Delta\lambda/2, \lambda + \Delta\lambda/2]$ and $[\beta - \Delta\beta/2, \beta + \Delta\beta/2]$. We can write the infinitesimal residence time in terms of the residence time density $\rho_j(\lambda, \beta)$ such that $dT_j(\lambda, \beta) = \rho_j(\lambda, \beta) d\lambda, d\beta$ and

$$\rho_j(\lambda, \beta) = \int_{-\infty}^{+\infty} dt \delta(\lambda_j(t) - \lambda) \delta(\beta_j(t) - \beta) \quad (\text{A1})$$

where we introduce the Dirac δ -function and $\lambda_j(t)$ and $\beta_j(t)$ represent the ecliptic longitude and latitude of the particle at time t respectively. The residence time of the particle within the extended range $\lambda_1 \leq \lambda < \lambda_2$ and $\beta_1 \leq \beta < \beta_2$ is then

$$T_j(\lambda_1, \lambda_2, \beta_1, \beta_2) = \int_{\lambda_1}^{\lambda_2} d\lambda \int_{\beta_1}^{\beta_2} d\beta \rho_j(\lambda, \beta). \quad (\text{A2})$$

The sky plane residence time density for a population of particles is the sum of the individual sky plane residence time densities

$$\rho(\lambda, \beta) = \sum_j \rho_j(\lambda, \beta) \quad (\text{A3})$$

Letting the normalization constant

$$C = \int d\lambda \int d\beta \rho(\lambda, \beta) \quad (\text{A4})$$

i.e. the cumulative time spent over the entire sky by all particles, the normalized residence time density is

$$\rho_N(\lambda, \beta) = \frac{1}{C} \rho(\lambda, \beta). \quad (\text{A5})$$

Thus, $\rho_N(\lambda, \beta)\Delta\lambda\Delta\beta$ is the fraction of time that all the particles spend within $(\Delta\lambda/2, \Delta\beta/2)$ of (λ, β) .

A.2. Sky plane number density

Let the particles' cumulative H -frequency distribution (HFD) be

$$N_{HFD}(H) = 10^{\alpha(H-H_1)} \quad (\text{A6})$$

i.e. $N_{HFD}(H)$ is the number of particles with absolute magnitude $< H$ and H_1 is therefore the absolute magnitude at which there is only one object in the population with $H < H_1$.

The differential HFD is then

$$n_{HFD}(H) dH = \alpha \ln 10 \, 10^{\alpha(H-H_1)} dH \quad (\text{A7})$$

i.e. there are $n_{HFD}(H) dH$ objects in the interval dH at magnitude H .

Since $\rho_N(\lambda, \beta)$ is the normalized sky plane residence time density, the differential sky plane number density of objects at absolute magnitude H is

$$n(\lambda, \beta, H) = n_{HFD}(H) \rho_N(\lambda, \beta). \quad (\text{A8})$$

i.e. the number of objects in an absolute magnitude interval of $[H - \Delta H/2, H + \Delta H/2]$ around H and in longitude λ and latitude β in the intervals $[\lambda - \Delta\lambda/2, \lambda + \Delta\lambda/2]$ and $[\beta - \Delta\beta/2, \beta + \Delta\beta/2]$ is $n(\lambda, \beta, H) \Delta\lambda \Delta\beta \Delta H$.

The cumulative sky plane number density of objects brighter than H_0 at (λ, β) is

$$\begin{aligned} N(\lambda, \beta, H_0) &= \int^{H_0} dH \, n(\lambda, \beta, H) \\ &= N_{HFD}(H_0) \rho_N(\lambda, \beta) \end{aligned} \quad (\text{A9})$$

so that the number of particles with $H < H_0$ in longitude and latitude intervals of widths $(\Delta\lambda, \Delta\beta)$ around (λ, β) is $N(\lambda, \beta, H_0) \Delta\lambda \Delta\beta$.

Thus, the number of particles with absolute magnitude $< H$ in the range $\lambda_1 \leq \lambda < \lambda_2$ and $\beta_1 \leq \beta < \beta_2$ is

$$\int_{\lambda_1}^{\lambda_2} d\lambda \int_{\beta_1}^{\beta_2} d\beta \, N(\lambda, \beta, H). \quad (\text{A10})$$

A.3. Optical Detection of TCOs

Following the nomenclature of §A.1, the sky plane residence time density for an individual particle j with absolute magnitude H_0 while it has apparent magnitude $V(H_0) < V_0$ and rate of motion $\omega < \omega_0$ is identical to eq. A1 except for a delimiter that constrains the rate of motion and apparent magnitude:

$$\rho_j^{vis}(\lambda, \beta, V_0, \omega_0, H_0) = \int_{-\infty}^{+\infty} dt \delta(\lambda_j(t) - \lambda) \delta(\beta_j(t) - \beta) \Big|_{V(H_0) < V_0, \omega < \omega_0} \quad (\text{A11})$$

The apparent magnitude V is calculated with the techniques described in Muinonen *et al.* (2010) and the rate of motion ω is determined by the plane of sky motion.

If all the particles have absolute magnitude H_0 their sky plane residence time density while they have $V(H_0) < V_0$ and $\omega < \omega_0$ is

$$\rho^{vis}(\lambda, \beta, V_0, \omega_0, H_0) = \sum_j \rho_j^{vis}(\lambda, \beta, V_0, \omega_0, H_0), \quad (\text{A12})$$

and their normalized sky plane residence time distribution density is:

$$\rho_N^{vis}(\lambda, \beta, V_0, \omega_0, H_0) = \frac{1}{C} \rho^{vis}(\lambda, \beta, V_0, \omega_0, H_0) \quad (\text{A13})$$

where the normalization constant C is from eq. A4. This normalization constant ensures that the normalized residence time in eq. A13 is the fraction of all possible particles, rather than the fraction of particles that satisfy the constraints, so that we can determine the number density of particles as derived below.

The number density of particles with $H < H_0$, $V(H_0) < V_0$ and $\omega < \omega_0$ as a function of sky plane location is (following the arguments in §A.2)

$$\begin{aligned} N^{vis}(\lambda, \beta, V_0, \omega_0, H_0) &= \int_{-\infty}^{+\infty} dH n(\lambda, \beta, V_0, \omega_0, H) \Big|_{V(H_0) < V_0, \omega < \omega_0} \\ &= \int_{-\infty}^{+\infty} dH n_{HFD}(H) \rho_N^{vis}(\lambda, \beta, V_0, \omega_0, H) \end{aligned} \quad (\text{A14})$$

$$(\text{A15})$$

i.e. There are $N^{vis}(\lambda, \beta, V_0, \omega_0, H_0) \Delta\lambda \Delta\beta$ particles in the range $[\lambda - \Delta\lambda/2, \lambda + \Delta\lambda/2]$ and with $[\beta - \Delta\beta/2, \beta + \Delta\beta/2]$ that also have $H < H_0$, $V(H_0) < V_0$ and $\omega < \omega_0$.

The total number of particles in the sky that have $V(H_0) < V_0$, $\omega < \omega_0$ and absolute magnitude brighter than H_0 is

$$= \int d\lambda \int d\beta N^{vis}(\lambda, \beta, V_0, \omega_0, H_0) \quad (\text{A16})$$

and the total number of particles in the range $\lambda_1 \leq \lambda < \lambda_2$ and $\beta_1 \leq \beta < \beta_2$ with the same constraints on V , ω and H is

$$= \int_{\lambda_1}^{\lambda_2} d\lambda \int_{\beta_1}^{\beta_2} d\beta N^{vis}(\lambda, \beta, V_0, \omega_0, H_0). \quad (\text{A17})$$

A.4. Infrared Detection of TCOs

We convert between diameter (D) and absolute magnitude using Fowler and Chillemi (1992):

$$\frac{D}{\text{meters}} = \frac{1.329 \times 10^6}{\sqrt{p_v}} 10^{-H/5} \quad (\text{A18})$$

where p_v is the albedo. We used $p_v = 0.11$ for the albedo throughout this work to make the conversion from absolute magnitude and diameter simple — $H = 18$ corresponds to 1 km diameter and factors of 10 changes in the diameter cause a change of 5 units in absolute magnitude.

The observed IR flux (F) for a particle at geocentric distance Δ and heliocentric distance r was calculated following Harris *et al.* (2009) and Mainzer *et al.* (2011):

$$F = \frac{\epsilon D^2}{4\Delta^2} \int_0^{2\pi} d\theta \int_0^{\frac{\pi}{2}} d\phi \int_{\lambda_1}^{\lambda_2} d\lambda B(\lambda, T_{ss}, \theta, \phi) \epsilon_b(\lambda) \sin \theta \cos \theta \quad (\text{A19})$$

where ϵ is a particle's thermal emissivity (we used 0.9 per Harris *et al.* 2009), θ and ϕ are the longitude and latitude on the object, ϵ_b is the passband efficiency as a function of

wavelength λ (not ecliptic longitude), B is the blackbody flux for an object with a sub-solar point temperature of T_{ss} . That temperature is given by

$$T_{ss} = \left[\frac{S(r) (1 - A)}{\eta \epsilon \sigma} \right]^{\frac{1}{4}} \quad (\text{A20})$$

where $S(r)$ is the solar flux at heliocentric distance r , η is the beaming parameter (we use $\eta = \pi$ for rapid rotators per Harris and Lagerros 2002), σ is the Stefan-Boltzmann constant, and A is the bond albedo.

We assume that TCOs are in thermal equilibrium because they are 1) small, in the range from ~ 0.1 m to ~ 1.0 m in diameter, 2) spend an average of about 9 months in Earth orbit with $r \sim 1$ au, and 3) rotate relatively quickly (see §A.6). *i.e.* there are no longitudinal or latitudinal variations in the blackbody flux emitted from the particle so that the function B in eq. A19 can be removed from the integral.

The technique for calculating the total number of particles in the sky plane and their observable properties in the infrared is analogous to the techniques outlined above for optical surveys except that the flux, F , is used instead of apparent magnitude and we use the diameter distribution instead of the absolute magnitude distribution.

A.5. Radar detection of TCOs

The sky plane residence time distribution and implementations with constraints are readily extended to the 4-dimensions relevant to radar surveys for TCOs in which a ground-based radar facility beams a radar signal and then searches for the reflected signal. In this case the 4-dimensions are the ecliptic longitude and latitude as well as the geocentric distance (range, Δ) and geocentric speed (range-rate, $\dot{\Delta}$).

The ratio between the received (P_{rec}) and transmitted (P_{tran}) signal power at Earth is

$$\frac{P_{rec}}{P_{tran}} = \frac{\epsilon_R A_R}{\Delta^4} \quad (\text{A21})$$

where ϵ_R is the radar facility’s detection efficiency and A_R is the particle’s radar albedo (the fraction of the signal at the particle reflected back to the transmitter). We use a radar albedo of 0.15 typical for S-type asteroids and NEOs ¹¹. The received power is detectable by the facility if it exceeds the intrinsic detector and background noise. However, the received power is spread over a range of wavelengths if the particle is rotating, further degrading the signal. The detected signal-to-noise ratio is then (Renzetti *et al.* 1988):

$$S/N = \frac{G_T G_A^2 \lambda^{\frac{5}{2}} A_R D \sqrt{NL}}{\Delta^4 k_b T_N \sqrt{32} \omega} \quad (\text{A22})$$

where G_T is the peak transmitter gain, G_A is the antenna gain, λ is the radar wavelength, D is the target diameter, N is the number of observations, k_b is Boltzmann’s constant, T_N is the system noise temperature, L is the integration time, and ω is the object’s rotation rate.

A.6. Meteoroid rotation rates

Rotation rates of meteoroid-scale objects (~ 0.1 to 1 m diameter) are essentially unknown. At the current time there is only one known NEO with $H \gtrsim 33$ (about 1 m diameter) and the smallest object in the Light Curve Database (LCDB, Warner *et al.* 2009) has $H \sim 29.5$ (the only known TCO, 2006 RH₁₂₀). The observational selection effects against identifying the fastest and slowest rotators must be tremendous for objects with $H \gtrsim 33$ *i.e.* the objects are so small that they are faint and require relatively long exposure times so that it is impossible to resolve fast rotation rates. Observations of fireballs add the

¹¹http://echo.jpl.nasa.gov/~lance/asteroid_radar_properties/nea.radaralbedo.html

complication of their interaction with the atmosphere and the associated ablation effects that may modify a meteoroid’s rotation rate (Beech and Brown 2000). Periodic variations in the flux along a meteor’s trail on an image might represent the object’s underlying rotation period but these observations will specifically select those objects with non-spherical shapes and fast rotation periods. Thus, there is not much that can be done to constrain the objects’ rotation rates except to use the available, limited and biased, observations.

Farinella *et al.* (1998) derived a spin period vs. diameter relationship of $T = 0.005 \frac{D}{\text{m}}$ hours for kilometer-scale asteroids. Extrapolating to the meteoroid size range yields periods of 18 s at 1 m diameter and 2 s at 10 cm diameter. While these rates seem fast, Beech and Brown (2000) point out that they are much slower than those observed for meteors in that size range. The meteor observations suggest a period-diameter relationship of $T \sim 0.0001 \frac{D}{\text{m}}$ hours — $50\times$ faster than that suggested by Farinella *et al.* (1998). Their results imply rotation periods of 0.5 s at 1 m diameter and 0.05 s at 10 cm diameter.

The Farinella *et al.* (1998) period vs. diameter relationship agrees well with the median values from the LCDB in the range from $[0, 100]$ m diameter as illustrated in fig. 14. We also fit the spin rates of the LCDB asteroids in the same intervals to Maxwellian distributions of the form:

$$f(\omega) = \sqrt{\frac{2}{\pi}} \frac{\omega^2}{\omega_0^3} \exp\left(-\frac{1}{2} \left[\frac{\omega}{\omega_0}\right]^2\right). \quad (\text{A23})$$

The Maxwellian distribution is the expected form of the rotation frequency distribution for a collisionally evolved asteroid population (*e.g.* Pravec *et al.* 2002) but the median value from our fits ($\hat{\omega} \approx 1.54 \omega_0$) is not a good representation of the predictions of Farinella *et al.* (1998) — they are typically faster than both the predicted and actual medians but approach the predicted frequency as the diameter decreases. Taken at face value it implies that the smaller objects (near 10 m diameter) have a more Maxwellian spin rate distribution but the distribution becomes less Maxwellian as the objects’ diameters increase (to 100 m diameter).

Pravec *et al.* (2008) have shown that the largest asteroids (many kilometers in diameter) have a Maxwellian spin-rate distribution but the spin-rates become less Maxwellian as their diameter decreases. Since this work is concerned only with the smallest asteroids and, motivated by the results in fig. 14, we assume that 1) the median rotation frequency ($\hat{\omega}$) of meteoroids in the $[0.1, 10]$ m diameter size range is given by Farinella *et al.* (1998) and 2) their spin-rate distribution is given by eq. A23 with $\omega_0 = \hat{\omega}/1.54$.

The smallest object for which a measured rotation period exists is the TCO 2006 RH₁₂₀ with a rotation period of 165 s (Kwiatkowski *et al.* 2009). The median rotation rate of objects of 2 m diameter corresponding to the size of 2006 RH₁₂₀ is about 1 s and 36 s using Beech and Brown (2000) and Farinella *et al.* (1998) respectively. With these medians the probability that a 2 m diameter object has a rotation period of ≥ 165 s in the two models is $\sim 1\%$ and $\sim 2.2 \times 10^{-5} \%$ respectively. Thus, 2006 RH₁₂₀'s rotation period would be a somewhat common $\sim 2.6 - \sigma$ event using our technique but a $5.2 - \sigma$ event if the asteroids in that size range had a median given by Beech and Brown (2000).

REFERENCES

- Ayers, W., R. McCrosky, and C. C.-Y. Shao 1970. Photographic observations of 10 artificial meteors. *SAO Spec. Rep #317* **317**, 40.
- Babadzhanov, P. B., and N. A. Konovalova 2004. *Astronomy and astrophysics* **428**(1).
- Baggaley, W. J. 2002. *Radar Observations*, Chapter 6. Cambridge Univ Press.
- Beech, M., and P. Brown 2000. Fireball flickering: the case for indirect measurement of meteoroid rotation rates. *Planet. Space Sci.* **48**, 925–932.
- Benner, L. A. M., M. C. Nolan, G. J. Black, J. D. Giorgini, J. L. Margot, P. Pravec, S. J. Ostro, and R. F. Jurgens 2002. Radar Images of Asteroid 38071 (1999 GU3). *Meteoritics and Planetary Science Supplement* **37**, 15.
- Boattini, A., E. C. Beshore, G. J. Garradd, A. R. Gibbs, A. D. Grauer, R. E. Hill, R. A. Kowalski, S. M. Larson, and R. H. McNaught 2008. 2008 TS26. *Minor Planet Electronic Circulars*, 119.
- Bottke, W. F., A. Morbidelli, R. Jedicke, J.-M. Petit, H. F. Levison, P. Michel, and T. S. Metcalfe 2002. Debaised Orbital and Absolute Magnitude Distribution of the Near-Earth Objects. *Icarus* **156**, 399–433.
- Bottke, W. F., Jr., A. Cellino, P. Paolicchi, and R. P. Binzel 2002. Asteroids III. *Asteroids III*.
- Bottke, W. F., Jr., D. Vokrouhlický, D. P. Rubincam, and D. Nesvorný 2006. The Yarkovsky and Yorp Effects: Implications for Asteroid Dynamics. *Annual Review of Earth and Planetary Sciences* **34**, 157–191.

- Britt, D. T., and G. J. Consolmagno 2004. Meteorite Porosities and Densities: A Review of Trends in the Data. In S. Mackwell and E. Stansbery (Eds.), *Lunar and Planetary Institute Science Conference Abstracts*, Volume 35 of *Lunar and Planetary Inst. Technical Report*, pp. 2108.
- Brown, P., S. Hunt, and S. Close 2001. Astronomical and physical data for meteoroids recorded by the altair radar. *Meteoroids 2001 Conference*.
- Brown, P., P. J. A. McCausland, M. Fries, E. Silber, W. N. Edwards, D. K. Wong, R. J. Weryk, J. Fries, and Z. Krzeminski 2011. The fall of the Grimsby meteorite-I: Fireball dynamics and orbit from radar, video, and infrasound records. *Meteoritics and Planetary Science* **46**, 339–363.
- Brown, P., R. E. Spalding, D. O. ReVelle, E. Tagliaferri, and S. P. Worden 2002. The flux of small near-Earth objects colliding with the Earth. *Nature* **420**, 294–296.
- Brown, P. G., R. Weryk, S. Kohut, W. N. Edwards, and Z. Krzemenski 2010. Development of an all-sky video meteor network in southern ontario, canada: The asgard system. *J. IMO* 38(1).
- Campbell, M. D., P. G. Brown, A. G. Leblanc, R. L. Hawkes, J. Jones, S. P. Worden, and R. R. Correll 2000. Image-intensified video results from the 1998 Leonid shower: I. Atmospheric trajectories and physical structure. *Meteoritics and Planetary Science* **35**, 1259–1267.
- Cepplecha, Z., J. Borovička, W. Elford, D. ReVelle, R. Hawkes, V. Poruban, M. Simek, and V. Porubcan 1998. Meteor phenomena and bodies. *Advances in Space Research* **84**.
- Cepplecha, Z., and R. McCrosky 1976. Fireball end heights: A diagnostic for the structure of meteoric material. *Journal of Geophysical Research* 81(35).

- Cepilecha, Z., and D. O. Revelle 2005. Fragmentation model of meteoroid motion, mass loss, and radiation in the atmosphere. *Meteoritics and Planetary Science* **40**, 35.
- Christensen, E., S. Larson, A. Boattini, A. Gibbs, A. Grauer, R. Hill, J. Johnson, R. Kowalski, and R. McNaught 2012. The Catalina Sky Survey: Current and Future Work. In *AAS/Division for Planetary Sciences Meeting Abstracts*, Volume 44 of *AAS/Division for Planetary Sciences Meeting Abstracts*.
- Chyba, M., G. Patterson, G. Picot, M. Granvik, R. Jedicke, and J. Vaubaillon 2014. Designing rendezvous missions with mini-moons using geometric optimal control. *Journal of Industrial and Management Optimization* **10**, 477–501.
- Denneau, L., R. Jedicke, T. Grav, M. Granvik, J. Kubica, A. Milani, P. Vereš, R. Wainscoat, D. Chang, F. Pierfederici, N. Kaiser, K. C. Chambers, J. N. Heasley, E. A. Magnier, P. A. Price, J. Myers, J. Kleyna, H. Hsieh, D. Farnocchia, C. Waters, W. H. Sweeney, D. Green, B. Bolin, W. S. Burgett, J. S. Morgan, J. L. Tonry, K. W. Hodapp, S. Chastel, S. Chesley, A. Fitzsimmons, M. Holman, T. Spahr, D. Tholen, G. V. Williams, S. Abe, J. D. Armstrong, T. H. Bressi, R. Holmes, T. Lister, R. S. McMillan, M. Micheli, E. V. Ryan, W. H. Ryan, and J. V. Scotti 2013. The Pan-STARRS Moving Object Processing System. *PASP* **125**, 357–395.
- Elvis, M., J. McDowell, J. A. Hoffman, and R. P. Binzel 2011. Ultra-low delta-v objects and the human exploration of asteroids. *Planet. Space Sci.* **59**, 1408–1412.
- Farinella, P., D. Vokrouhlicky, and W. K. Hartmann 1998. Erratum: Meteorite Delivery via Yarkovsky Orbital Drift [Volume 132, Number 2, pages 378-387 (1998)]. *Icarus* **134**, 347.
- Fowler, J., and J. Chillemi 1992. Subaru Lightcurve Observations of Sub-km-Sized

- Main-Belt Asteroids. In *The IRAS Minor Planet Survey* (E. F. Tedesco, ed.) **Tech. Rpt. PL-TR-92-2049**, 17–43.
- Granvik, M., R. Jedicke, B. Bolin, M. Chyba, and G. Patterson 2013. *Earth’s Temporarily-Captured Natural Satellites - The First Step towards Utilization of Asteroid Resources*, pp. 151–167.
- Granvik, M., J. Vaubaillon, and R. Jedicke 2012. The population of natural Earth satellites. *Icarus* **218**, 262–277.
- Greenstreet, S., and B. Gladman 2012. High-inclination Atens ARE Rare. In *AAS/Division for Planetary Sciences Meeting Abstracts*, Volume 44 of *AAS/Division for Planetary Sciences Meeting Abstracts*, pp. 305.05.
- Harris, A., and J. Lagerros 2002. Asteroids in the Thermal Infrared. *Asteroids III*.
- Harris, A. W., M. Mueller, C. M. Lisse, and A. F. Cheng 2009. A survey of Karin cluster asteroids with the Spitzer Space Telescope. *Icarus* **199**, 86–96.
- Hawkes, R. 2002. *Radar Observations*, Chapter 5. Cambridge Univ Press.
- Hunt, S., M. Oppenheim, S. Close, P. Brown, F. McKeen, and M. Minardi 2004. Determination of the meteoroid velocity distribution at the earth using high-gain radar. *Icarus* **168**(1).
- Ivezic, Z., T. Axelrod, W. N. Brandt, D. L. Burke, C. F. Claver, A. Connolly, K. H. Cook, P. Gee, D. K. Gilmore, S. H. Jacoby, R. L. Jones, S. M. Kahn, J. P. Kantor, V. V. Krabbendam, R. H. Lupton, D. G. Monet, P. A. Pinto, A. Saha, T. L. Schalk, D. P. Schneider, M. A. Strauss, C. W. Stubbs, D. Sweeney, A. Szalay, J. J. Thaler, J. A. Tyson, and LSST Collaboration 2008. Large Synoptic Survey Telescope: From Science Drivers To Reference Design. *Serbian Astronomical Journal* **176**, 1–13.

- Jedicke, R. 1996. Detection of Near Earth Asteroids Based Upon Their Rates of Motion. *AJ* **111**, 970.
- Jedicke, R., J. Larsen, and T. Spahr 2002. Observational Selection Effects in Asteroid Surveys. *Asteroids III*, 71–87.
- Jenniskens, P., P. S. Gural, L. Dynneson, B. J. Grigsby, K. E. Newman, M. Borden, M. Koop, and D. Holman 2011. CAMS: Cameras for Allsky Meteor Surveillance to establish minor meteor showers. *Icarus* **216**, 40–61.
- Jenniskens, P., M. H. Shaddad, D. Numan, S. Elsir, A. M. Kudoda, M. E. Zolensky, L. Le, G. A. Robinson, J. M. Friedrich, D. Rumble, A. Steele, S. R. Chesley, A. Fitzsimmons, S. Duddy, H. H. Hsieh, G. Ramsay, P. G. Brown, W. N. Edwards, E. Tagliaferri, M. B. Boslough, R. E. Spalding, R. Dantowitz, M. Kozubal, P. Pravec, J. Borovicka, Z. Charvat, J. Vaubaillon, J. Kuiper, J. Albers, J. L. Bishop, R. L. Mancinelli, S. A. Sandford, S. N. Milam, M. Nuevo, and S. P. Worden 2009. The impact and recovery of asteroid 2008 TC₃. *Nature* **458**, 485–488.
- Jenniskens, P., J. Vaubaillon, R. P. Binzel, F. E. DeMeo, D. Nesvorný, W. F. Bottke, A. Fitzsimmons, T. Hiroi, F. Marchis, J. L. Bishop, P. Vernazza, M. E. Zolensky, J. S. Herrin, K. C. Welten, M. M. M. Meier, and M. H. Shaddad 2010. Almahata Sitta (=asteroid 2008 TC₃) and the search for the ureilite parent body. *Meteoritics and Planetary Science* **45**, 1590–1617.
- Jones, J., P. G. Brown, K. J. Ellis, A. Webster, M. D. Campbell-Brown, Z. Krzeminski, and R. Weryk 2005. The canadian meteor orbit radar : system overview and preliminary results. *Planetary and Space Science* **53**.
- Kero, J., C. Szasz, A. Pellinen-Wannberg, G. Wannberg, and A. Westman 2005. Power

- fluctuations in meteor head echoes observed with the eiscat vhf radar. *Earth, Moon, and Planets* **95**(1-4).
- Kessler, D., P. Landry, J. Gabbard, and J. Moran 1980. *Ground radar detection of meteoroids in space*. IAU.
- Knott, E., J. Shaeffer, and T. Michael 2004. *RADAR Cross Section*. SciTech Publishing, Inc.
- Kwiatkowski, T., A. Kryszczyńska, M. Polińska, D. A. H. Buckley, D. O’Donoghue, P. A. Charles, L. Crause, S. Crawford, Y. Hashimoto, A. Kniazev, N. Loaring, E. Romero Colmenero, R. Sefako, M. Still, and P. Vaisanen 2009. Photometry of 2006 RH₁₂₀: an asteroid temporary captured into a geocentric orbit. *A&A* **495**, 967–974.
- Larson, S., J. Brownlee, C. Hergenrother, and T. Spahr 1998. The Catalina Sky Survey for NEOs. In *Bulletin of the American Astronomical Society*, Volume 30 of *Bulletin of the American Astronomical Society*, pp. 1037.
- Mainzer, A., J. Bauer, T. Grav, J. Masiero, R. M. Cutri, J. Dailey, P. Eisenhardt, R. S. McMillan, E. Wright, R. Walker, R. Jedicke, T. Spahr, D. Tholen, R. Alles, R. Beck, H. Brandenburg, T. Conrow, T. Evans, J. Fowler, T. Jarrett, K. Marsh, F. Masci, H. McCallon, S. Wheelock, M. Wittman, P. Wyatt, E. DeBaun, G. Elliott, D. Elsbury, T. Gautier, IV, S. Gomillion, D. Leisawitz, C. Maleszewski, M. Micheli, and A. Wilkins 2011. Preliminary Results from NEOWISE: An Enhancement to the Wide-field Infrared Survey Explorer for Solar System Science. *ApJ* **731**, 53.
- Mainzer, A., T. Grav, J. Masiero, J. Bauer, E. Wright, R. M. Cutri, R. S. McMillan, M. Cohen, M. Ressler, and P. Eisenhardt 2011. Thermal Model Calibration for Minor Planets Observed with Wide-field Infrared Survey Explorer/NEOWISE. *ApJ* **736**, 100.

- Mainzer, A., J. Masiero, T. Grav, J. Bauer, D. J. Tholen, R. S. McMillan, E. Wright, T. Spahr, R. M. Cutri, R. Walker, W. Mo, J. Watkins, E. Hand, and C. Maleszewski 2012. NEOWISE Studies of Asteroids with Sloan Photometry: Preliminary Results. *ApJ* **745**, 7.
- Mainzer, A. K. 2006. NEOCam: The Near-Earth Object Camera. In *AAS/Division for Planetary Sciences Meeting Abstracts #38*, Volume 38 of *Bulletin of the American Astronomical Society*, pp. 568.
- McMurtry, C., D. Lee, J. Beletic, C.-Y. A. Chen, R. T. Demers, M. Dorn, D. Edwall, C. Bacon Fazar, W. J. Forrest, F. Liu, A. K. Mainzer, J. L. Pipher, and A. Yulius 2013. Development of sensitive long-wave infrared detector arrays for passively cooled space missions. *ArXiv e-prints*.
- Micheli, M., D. J. Tholen, and G. T. Elliott 2013. 2012 LA, an optimal astrometric target for radiation pressure detection. *Icarus* **226**, 251–255.
- Monet, D. G., T. Axelrod, T. Blake, C. F. Claver, R. Lupton, E. Pearce, R. Shah, and D. Woods 2013. Rapid Cadence Collections with the Space Surveillance Telescope. In *American Astronomical Society Meeting Abstracts*, Volume 221 of *American Astronomical Society Meeting Abstracts*, pp. 352.17.
- Morbidelli, A., and D. Vokrouhlický 2003. The Yarkovsky-driven origin of near-Earth asteroids. *Icarus* **163**, 120–134.
- Moskovitz, N., T. Endicott, T. Lister, B. Ryan, E. Ryan, M. Willman, C. Hergenrother, R. Binzel, D. Polishook, F. DeMeo, S. Benecchi, S. Sheppard, F. Marchis, T. Angusteijn, P. Birthwhistle, A. Verveer, A. Gulbis, T. Nagayama, A. Gilmore, and P. Kilmartin 2013. The Near-Earth Flyby of Asteroid 2012 DA14. In *AAS/Division*

for Planetary Sciences Meeting Abstracts, Volume 45 of *AAS/Division for Planetary Sciences Meeting Abstracts*, pp. 101.03.

Muinonen, K., I. N. Belskaya, A. Cellino, M. Delbò, A.-C. Levasseur-Regourd, A. Penttilä, and E. F. Tedesco 2010. A three-parameter magnitude phase function for asteroids. *Icarus* **209**, 542–555.

Murray, N., J. C. Weingartner, and C. Capobianco 2004. On the flux of extrasolar dust in earths atmosphere. *Astrophysical Journal* **600**.

Musci, R., R. Weryk, P. Brown, M. D. Campbell-Brown, and P. a. Wiegert 2012. An optical survey for millimeter-sized interstellar meteoroids. *The Astrophysical Journal* *745*(2), 161.

Popova, O., J. Borovička, W. K. Hartmann, P. Spurný, E. Gnos, I. Nemtchinov, and J. M. Trigo-Rodríguez 2011. Very low strengths of interplanetary meteoroids and small asteroids. *Meteoritics and Planetary Science* **46**, 1525–1550.

Pravec, P., A. W. Harris, and T. Michalowski 2002. Asteroid Rotations. In W. Bottke, A. Cellino, P. Paolicchi, and R. P. Binzel (Eds.), *Asteroids III*, pp. 113–122. University of Arizona Press.

Pravec, P., A. W. Harris, D. Vokrouhlický, B. D. Warner, P. Kušnirák, K. Hornoch, D. P. Pray, D. Higgins, J. Oey, A. Galád, Š. Gajdoš, L. Kornoš, J. Világi, M. Husárik, Y. N. Krugly, V. Shevchenko, V. Chiorny, N. Gaftonyuk, W. R. Cooney, J. Gross, D. Terrell, R. D. Stephens, R. Dyvig, V. Reddy, J. G. Ries, F. Colas, J. Lecacheux, R. Durkee, G. Masi, R. A. Koff, and R. Goncalves 2008. Spin rate distribution of small asteroids. *Icarus* **197**, 497–504.

Renzetti, N. A., T. W. Thompson, and M. A. Slade 1988. Relative planetary radar

- sensitivities: Arecibo and Goldstone. In E. C. Posner (Ed.), *The Telecommunications and Data Acquisition Report*, pp. 287–293.
- Sarma, T., and J. Jones 1985. Double-station observations of 454 TV meteors. I - Trajectories. *Bulletin of the Astronomical Institutes of Czechoslovakia* **36**, 9–24.
- Schwan 1995. *Proceedings of the 1995 Space Surveillance Workshop.*, Volume <http://www.dtic.mil/cgi-bin/GetTRDoc?AD=ADA294240>, pp. 106. Lincoln Laboratory.
- Spurný, P., J. Borovička, and L. Shrbený 2007. Automation of the Czech part of the European fireball network: equipment, methods and first results. In G. B. Valsecchi, D. Vokrouhlický, and A. Milani (Eds.), *IAU Symposium*, Volume 236 of *IAU Symposium*, pp. 121–130.
- Stokely, C. L., E. G. Stansbery, and R. M. Goldstein 2009. Debris flux comparisons from the Goldstone Radar, Haystack Radar, and Hax Radar prior, during, and after the last solar maximum. *Advances in Space Research* **44**, 364–370.
- Stokes, G. H., J. B. Evans, H. E. M. Viggh, F. C. Shelly, and E. C. Pearce 2000. Lincoln Near-Earth Asteroid Program (LINEAR). *Icarus* **148**, 21–28.
- Takada, M. 2010. Subaru Hyper Suprime-Cam Project. In N. Kawai and S. Nagataki (Eds.), *American Institute of Physics Conference Series*, Volume 1279 of *American Institute of Physics Conference Series*, pp. 120–127.
- Tingay, S. J., D. L. Kaplan, B. McKinley, F. Briggs, R. B. Wayth, N. Hurley-Walker, J. Kennewell, C. Smith, K. Zhang, W. Arcus, N. D. R. Bhat, D. Emrich, D. Herne, N. Kudryavtseva, M. Lynch, S. M. Ord, M. Waterson, D. G. Barnes, M. Bell, B. M. Gaensler, E. Lenc, G. Bernardi, L. J. Greenhill, J. C. Kasper, J. D. Bowman,

- D. Jacobs, J. D. Bunton, L. deSouza, R. Koenig, J. Pathikulangara, J. Stevens, R. J. Cappallo, B. E. Corey, B. B. Kincaid, E. Kratzenberg, C. J. Lonsdale, S. R. McWhirter, A. E. E. Rogers, J. E. Salah, A. R. Whitney, A. Deshpande, T. Prabu, N. Udaya Shankar, K. S. Srivani, R. Subrahmanyam, A. Ewall-Wice, L. Feng, R. Goeke, E. Morgan, R. A. Remillard, C. L. Williams, B. J. Hazelton, M. F. Morales, M. Johnston-Hollitt, D. A. Mitchell, P. Procopio, J. Riding, R. L. Webster, J. S. B. Wyithe, D. Oberoi, A. Rosh, R. J. Sault, and A. Williams 2013. On the Detection and Tracking of Space Debris Using the Murchison Widefield Array. I. Simulations and Test Observations Demonstrate Feasibility. *AJ* **146**, 103.
- Tokunaga, A. T., and R. Jedicke 2007. *New Generation Ground-Based Optical/Infrared Telescopes*, pp. 719–734.
- Tonry, J. L. 2011. An Early Warning System for Asteroid Impact. *PASP* **123**, 58–73.
- Vereš, P., R. Jedicke, L. Denneau, R. Wainscoat, M. J. Holman, and H. Lin 2012. Improved Asteroid Astrometry and Photometry with Trail Fitting. *PASP*.
- Verniani, F. 1973. An analysis of the physical parameters of 5759 faint radio meteors. *Journal of Geophysical Research* **78**(35).
- Wainscoat, R. J., P. Veres, B. Bolin, L. Denneau, R. Jedicke, M. Micheli, and S. Chastel 2013. The Pan-STARRS search for Near Earth Objects: recent progress and future plans. In *AAS/Division for Planetary Sciences Meeting Abstracts*, Volume 45 of *AAS/Division for Planetary Sciences Meeting Abstracts*.
- Warner, B. D., A. W. Harris, and P. Pravec 2009. The asteroid lightcurve database. *Icarus* **202**, 134–146.
- Weryk, R. J., and P. G. Brown 2013. Simultaneous radar and video meteors-II: Photometry and ionisation. *Planet. Space Sci.* **81**, 32–47.

- Weryk, R. J., M. D. Campbell-Brown, P. A. Wiegert, P. Brown, P. Gural, and R. Hawkes 2008. Meteoroid Fragmentation as seen by the Canadian Automated Meteor Observatory (CAMO). In *AAS/Division for Planetary Sciences Meeting Abstracts #40*, Volume 40 of *Bulletin of the American Astronomical Society*, pp. 455.
- Weryk, R. J., M. D. Campbell-Brown, P. A. Wiegert, P. G. Brown, Z. Krzeminski, and R. Musci 2013. The Canadian Automated Meteor Observatory (CAMO): System overview. *Icarus* **225**, 614–622.
- Wright, E. L., P. R. M. Eisenhardt, A. K. Mainzer, M. E. Ressler, R. M. Cutri, T. Jarrett, J. D. Kirkpatrick, D. Padgett, R. S. McMillan, M. Skrutskie, S. A. Stanford, M. Cohen, R. G. Walker, J. C. Mather, D. Leisawitz, T. N. Gautier, III, I. McLean, D. Benford, C. J. Lonsdale, A. Blain, B. Mendez, W. R. Irace, V. Duval, F. Liu, D. Royer, I. Heinrichsen, J. Howard, M. Shannon, M. Kendall, A. L. Walsh, M. Larsen, J. G. Cardon, S. Schick, M. Schwalm, M. Abid, B. Fabinsky, L. Naes, and C.-W. Tsai 2010. The Wide-field Infrared Survey Explorer (WISE): Mission Description and Initial On-orbit Performance. *AJ* **140**, 1868–1881.

Survey	Type	FOR (deg ²)	T_{exp} (s)	V_{lim}	ω_{lim} °/d	N_{sky}	N_{TCO} TCO/d	τ_{ref} d
PS1 ¹	wide-area	1,000	40	21.7	3	0.03	0.013	2.3
ATLAS ²	all-sky	20,000	30	20.0	15	0.0084	0.01	0.8
SST ³	all-sky	20,000	5	22.0	20	0.4	0.02	18.0
LSST ⁴	wide-area	7,000	15	24.7	10	8.5	0.27	31.0
Subaru-HSC ⁵	targeted	450	15	24.5	1.0	0.4 [†]	0.05	8.0
CAMO ⁶	meteor	20,000	N/A	7.5	N/A	~ 0	N/A	N/A
CAMS ⁷	meteor	20,000	0.017	4.8	11,300	~ 0	0.04	26.1

Table 1: TCO detection performance for seven optical surveys. For the first five telescopic surveys we consider only TCOs with absolute magnitude $H < 38$ corresponding roughly to those > 10 cm diameter. FOR is the Field-of-Regard — the total average amount of sky surveyed each night in a mode suitable for identifying TCOs. V_{lim} and ω_{lim} are the survey’s limiting V -band magnitude and approximate rate of motion. N_{sky} and N_{TCO} are the number of TCOs on the sky that are detectable by the survey at any instant and the average number of TCOs detectable by the survey per day. τ_{ref} is the refresh rate for the observable TCOs, equivalent to their average observable lifetime.

¹Denneau *et al.* (2013)

²Tonry (2011)

³Monet *et al.* (2013)

⁴Ivezic *et al.* (2008)

⁵Takada (2010)

⁶Weryk *et al.* (2008)

⁷Jenniskens *et al.* (2011)

[†]In this case only, the number of TCOs detectable by the HSC survey in one night.

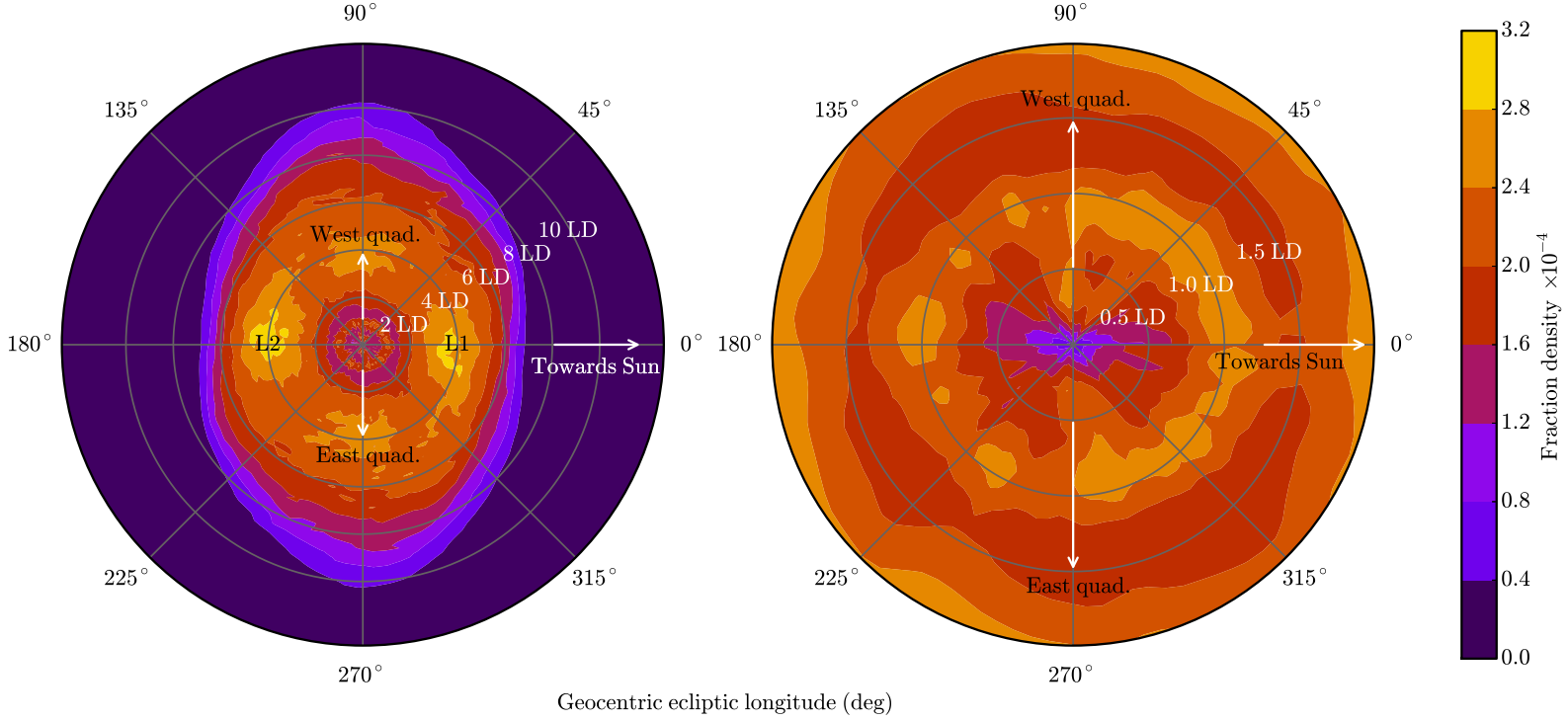


Fig. 1.— Normalized geocentric TCO $\Delta - \theta$ residence density distribution (eq. A5) with no restrictions on apparent magnitude or rate of motion where Δ is the geocentric distance and θ is the azimuthal angle about the ecliptic pole with the origin in the sunward direction. The panel on the right is a magnified version of the panel on the left for $\Delta < 2$ LD. The Sun is to the right in both panels *i.e.* at 0°. The number of objects in the Δ - θ range, $(\Delta \pm d\Delta/2, \theta \pm d\theta/2)$, is the product of the fraction density and $(d\Delta, d\theta)$.

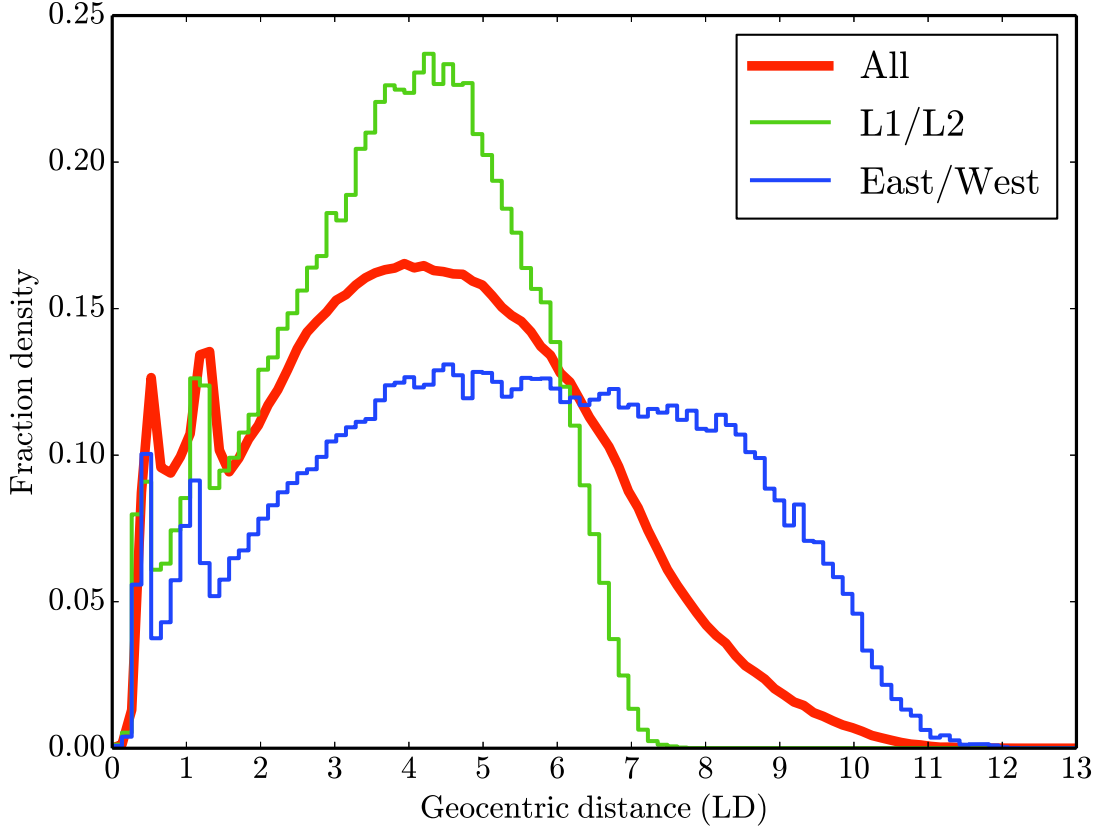


Fig. 2.— Geocentric distance distribution in lunar distances (~ 0.00257 au) for all TCOs (thick black line), near the L2 and L1 Lagrange points (light gray line), and near the two quadratures (dark gray line). ‘Near’ means within 15° in longitude and within 10° in latitude. The number of objects in the geocentric distance range $(\Delta \pm d\Delta/2)$ is the product of the fraction density and $d\Delta$.

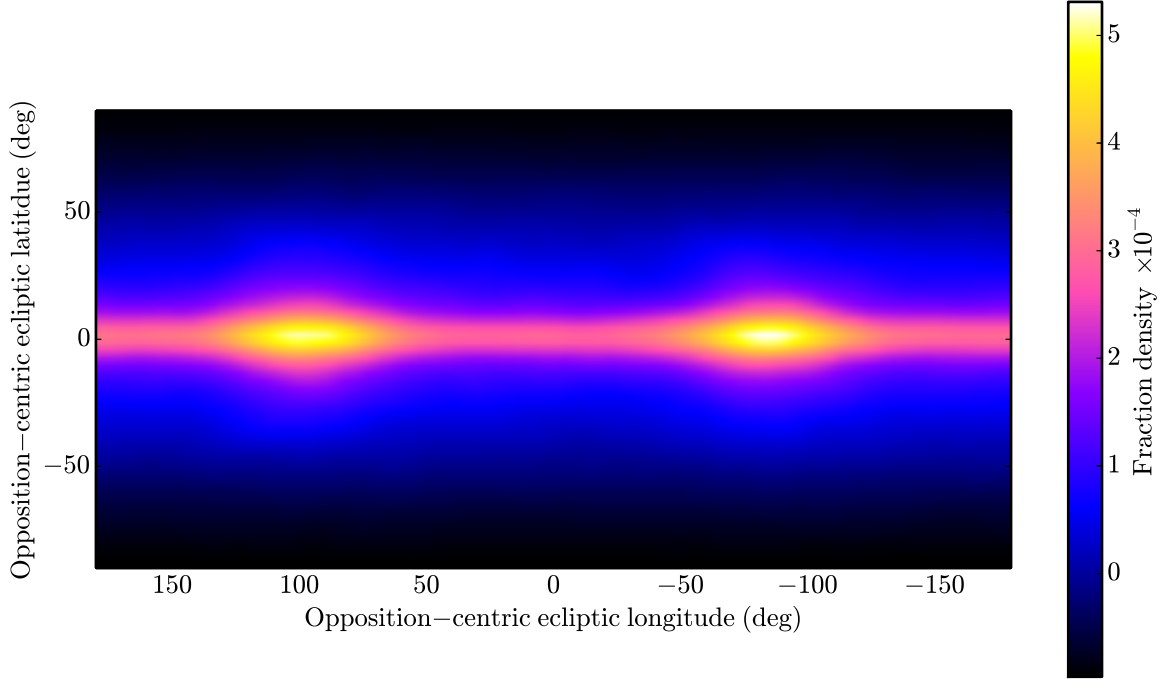


Fig. 3.— Normalized geocentric TCO sky plane residence density distribution (eq. A5) with no restrictions on apparent magnitude or rate of motion in an opposition-centric ecliptic reference system. Negative opposition-centric longitudes are west of opposition. The values are the fraction of the population in $3^\circ \times 3^\circ$ bins. The number of objects in the opposition-centric longitude and latitude range, $(\lambda \pm d\lambda/2, \beta \pm d\beta/2)$, is the product of the fraction density and $(d\lambda, d\beta)$.

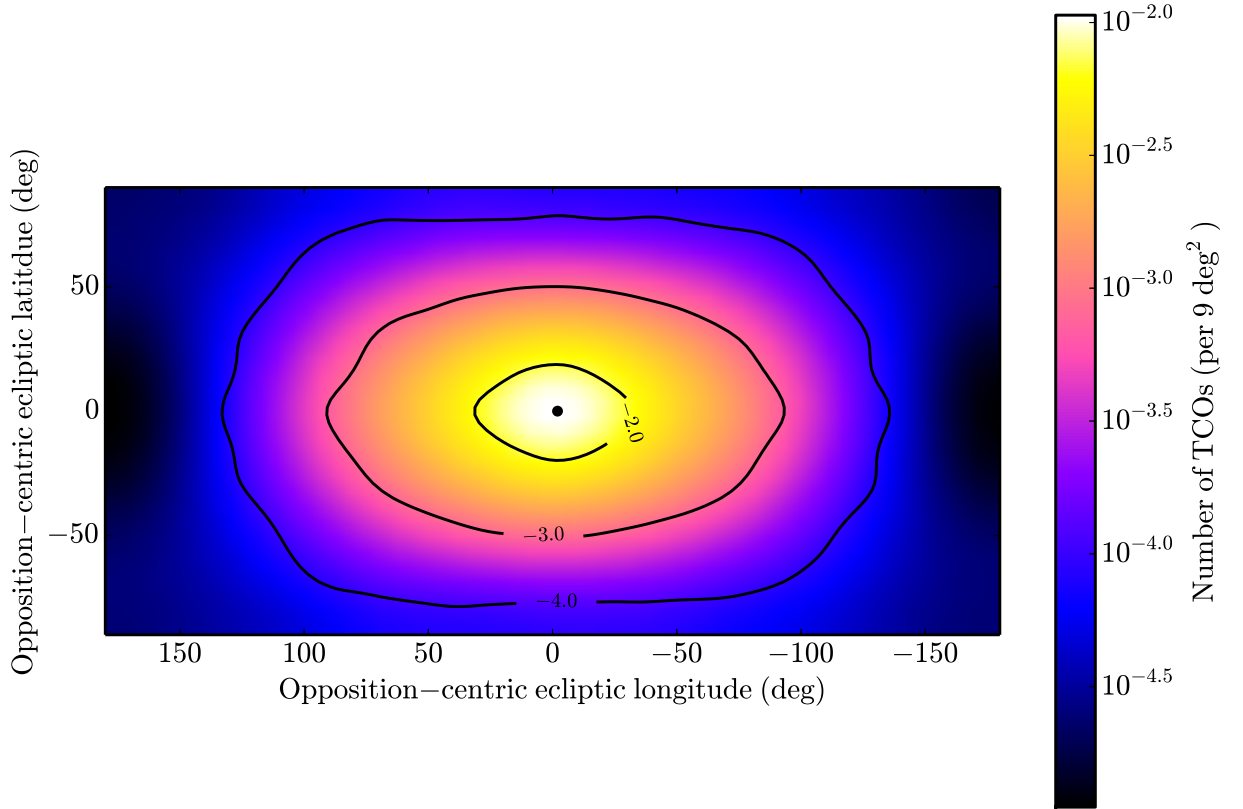


Fig. 4.— Sky plane number density of TCOs with $H < 38$ (~ 10 cm diameter), apparent magnitude $V < 20$ and rate of motion $< 15^\circ/\text{d}$. The constraints are roughly consistent with the expected performance characteristics of the ATLAS system (Tonry 2011) but are generally applicable to any telescopic TCO survey except for (roughly) a normalization constant. The small black circle in the center represents the size of Earth’s umbra and penumbra at 4 lunar distances. The values are the number of TCOs in $3^\circ \times 3^\circ$ bins.

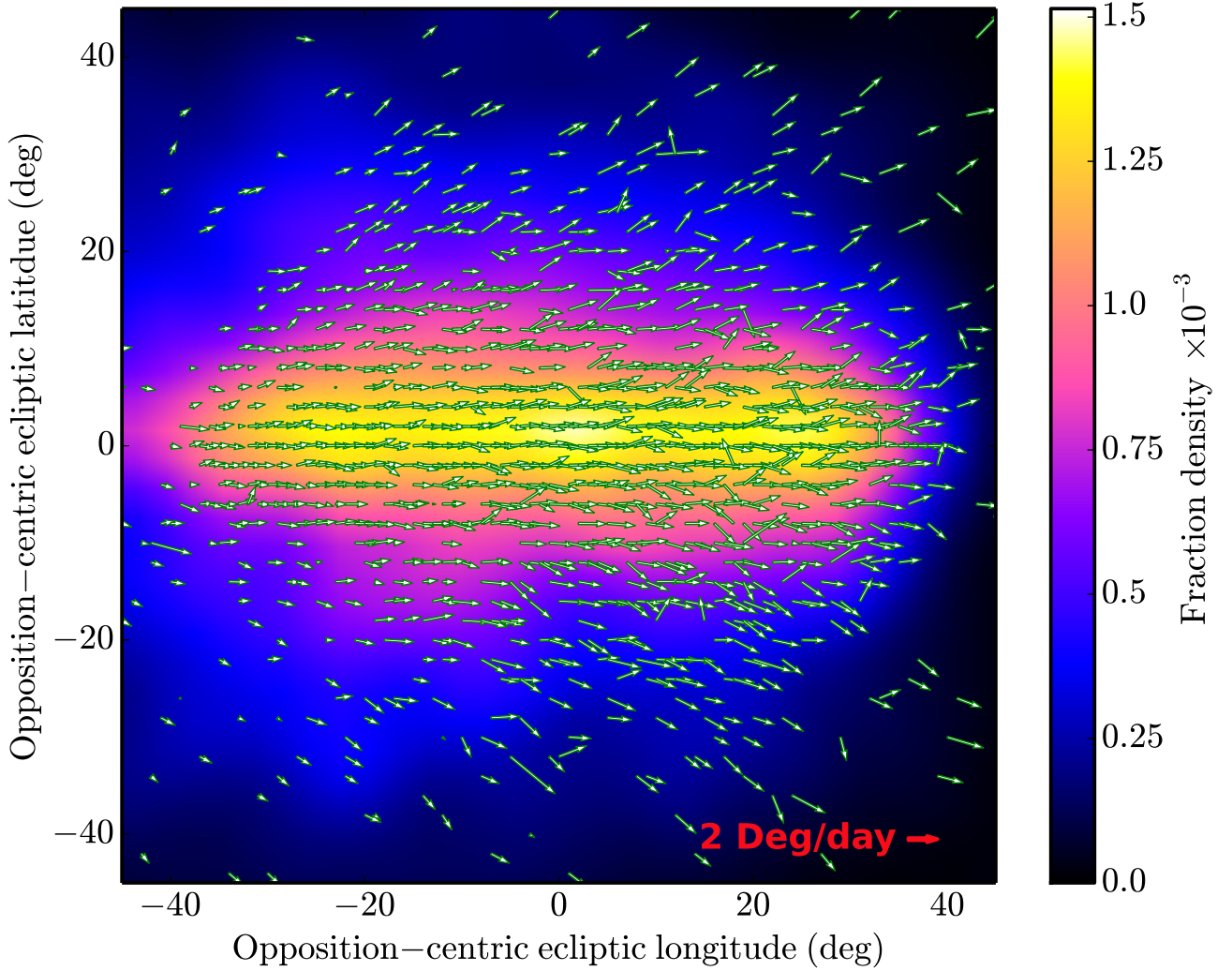


Fig. 5.— Sky plane distribution of TCOs at the moment of capture near L2 without constraints on the apparent magnitude or rate of motion. The contour values are the fraction of the population at capture in the $3^\circ \times 3^\circ$ bins. The vectors represent the average rate of motion and direction of the TCOs in the bins at the time of capture. A vector representing a $2^\circ/\text{d}$ rate of motion is shown in the lower right. The number of objects in the opposition-centric longitude and latitude range, $(\lambda \pm d\lambda/2, \beta \pm d\beta/2)$, is the product of the fraction density and $(d\lambda, d\beta)$.

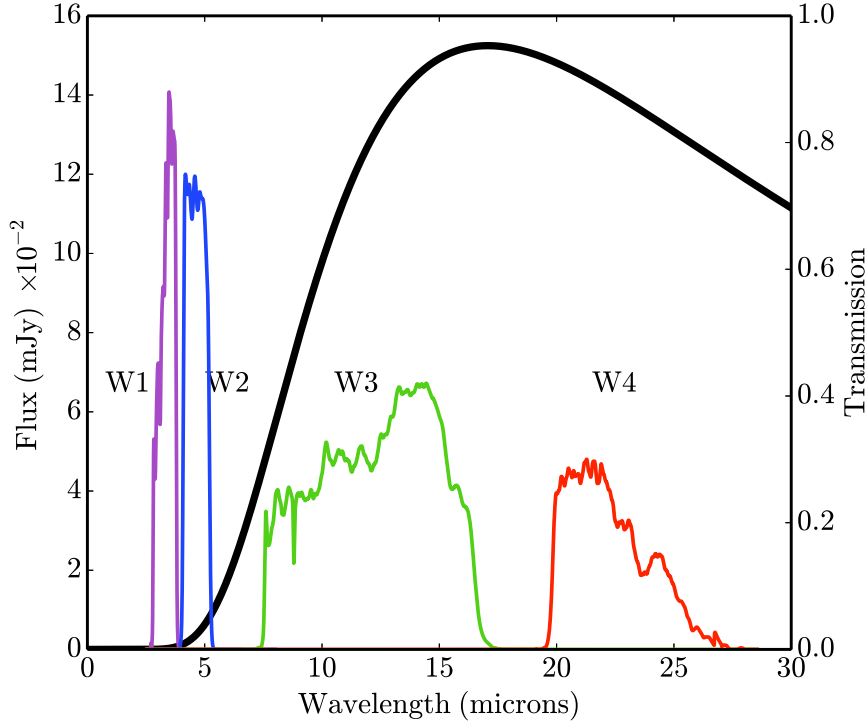


Fig. 6.— The thick solid line represents the IR flux (left axis) for a 1 meter diameter mini-moon at 300 K at 4 LD from the observer. (Details of the TCO IR flux calculation are provided in A.4) The thinner curves illustrate the transmission percentages (right axis) for the 4 WISE pass bands (from <http://www.astro.ucla.edu/~wright/WISE/passbands.html>).

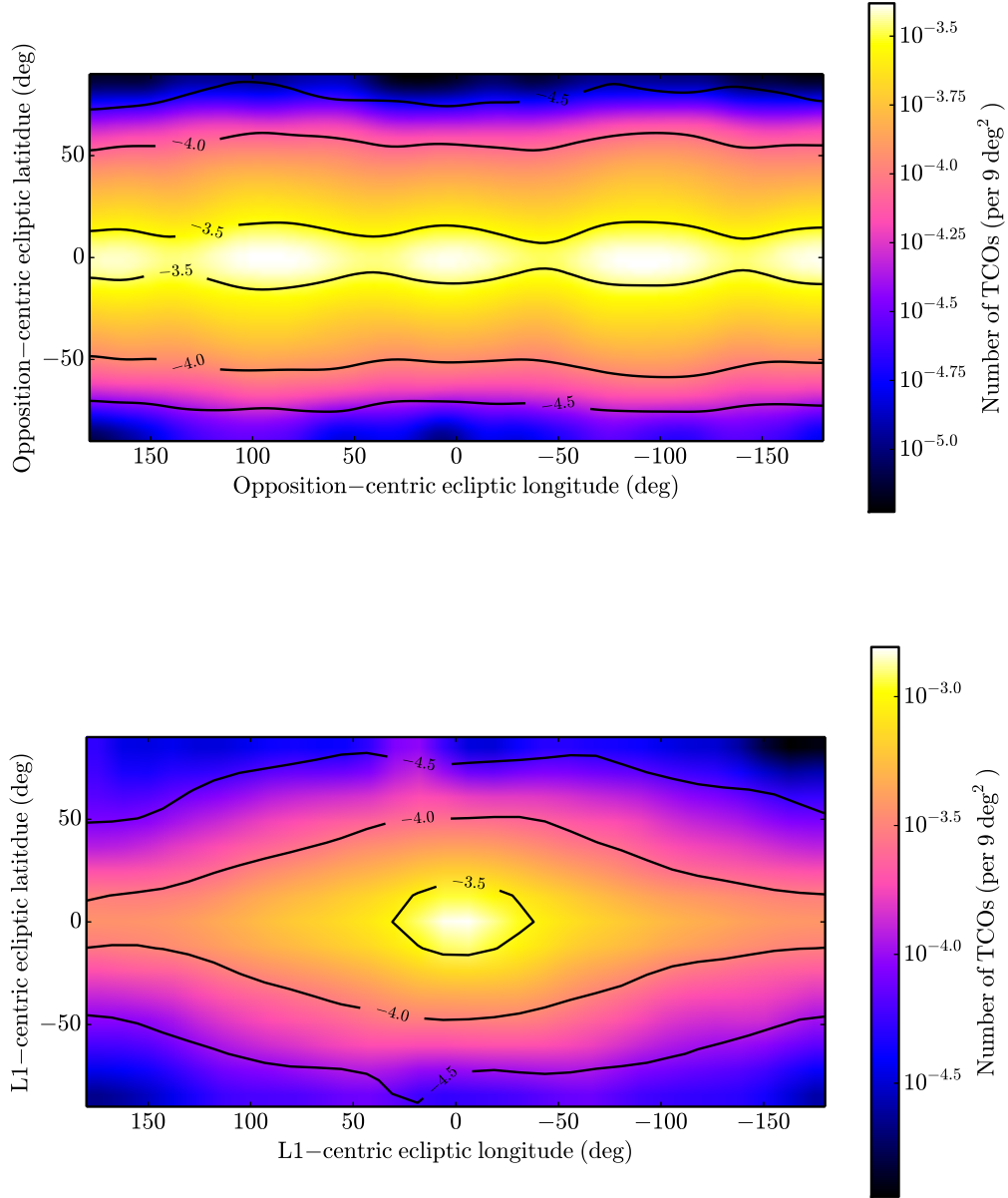


Fig. 7.— Geocentric TCO sky plane number distribution in WISE’s 12 micron W3 band for TCOs with flux > 0.65 mJy from (top) geocenter and moving at $< 3^\circ/\text{d}$ and (bottom) from a spacecraft with a 0.5 meter aperture mirror at the Earth-Sun L1 Lagrange point capable of detecting TCOs moving at $< 10^\circ/\text{d}$. The center of the figure is in the direction of Earth as viewed from L1.

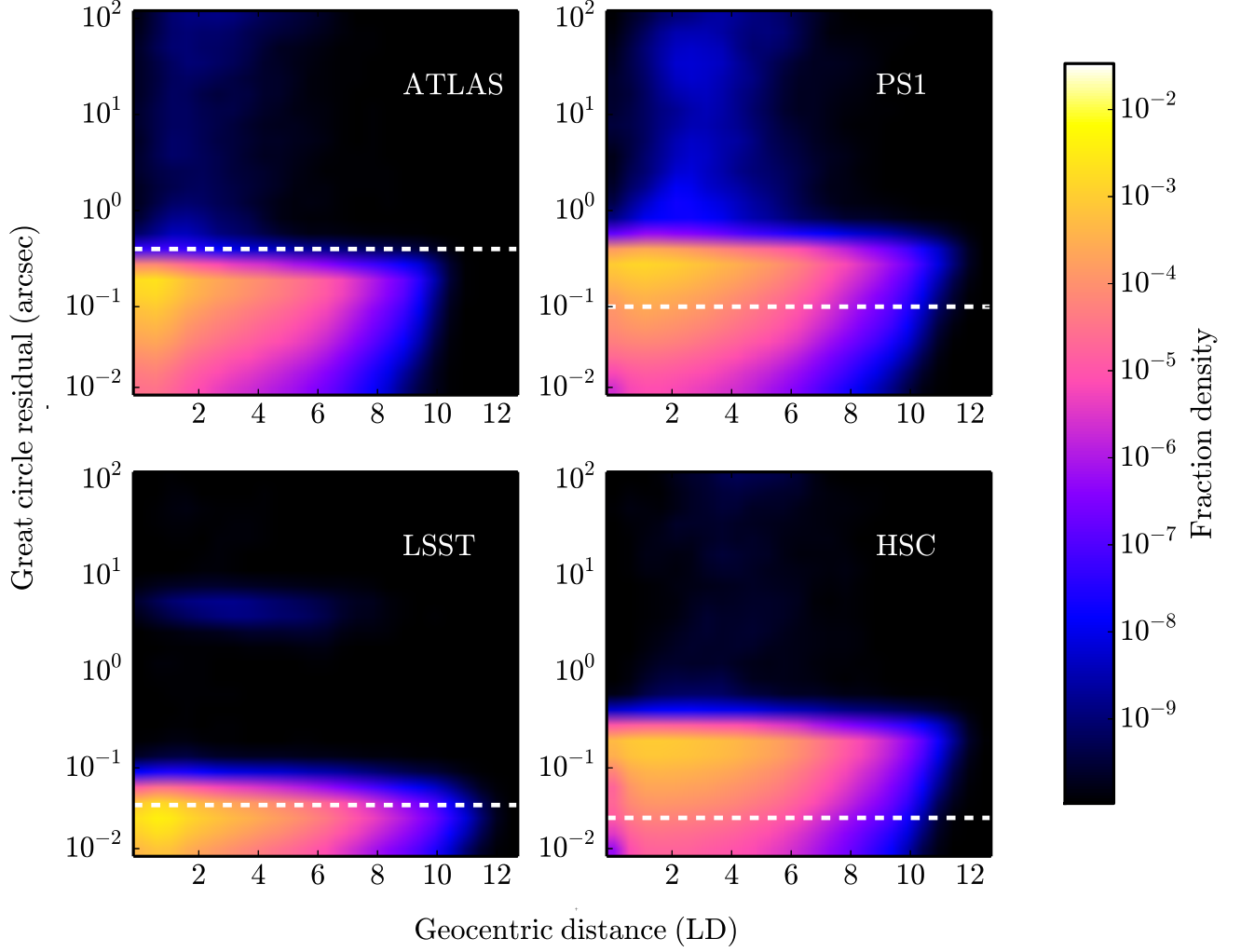


Fig. 8.— True GCR versus geocentric distance for TCOs detectable with the ATLAS, PS1, HSC and LSST optical surveys. The GCRs were calculated for the typical or expected number of exposures (3,4,3,2) and total time between first and last exposures of (40 min, 60 min, 40 min, 60 min) for (ATLAS, PS1, HSC, LSST) respectively. The dashed white lines provide a rough estimate for the astrometric uncertainty typical of each survey at $S/N=5$ given by the (pixel scale)/5. The number of objects in the $GCR \pm dGCR/2$, $\Delta \pm d\Delta/2$, is the product of the fraction density and $(dGCR, d\Delta)$.

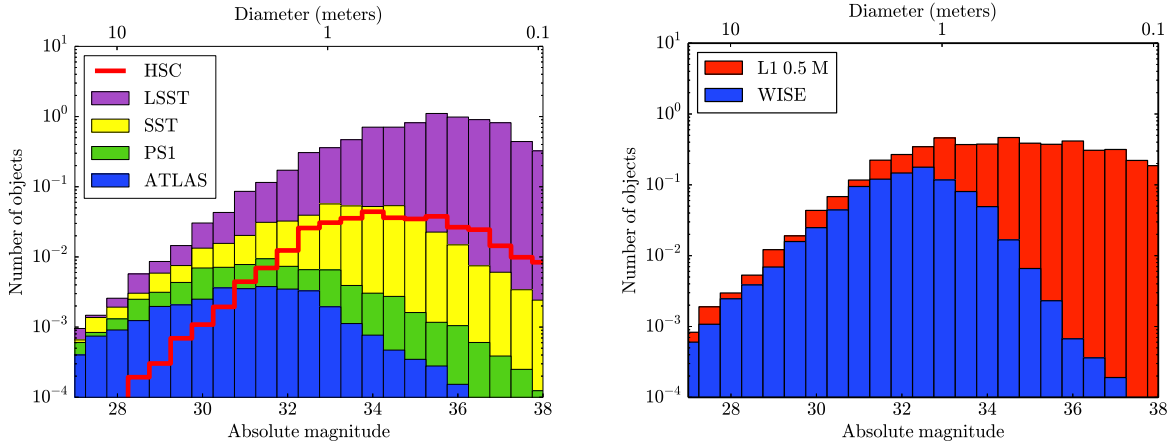


Fig. 9.— Size distribution of detectable TCOs for (left) four different ground-based optical surveys as described in §3.1 and (right) two different space-based IR surveys as described in §4. Each bin represents the number of TCOs per 0.5 absolute magnitude on the entire sky detectable by the survey. *i.e.* it is not corrected for the survey’s sky coverage or cadence. Survey capabilities are provided in table 1.

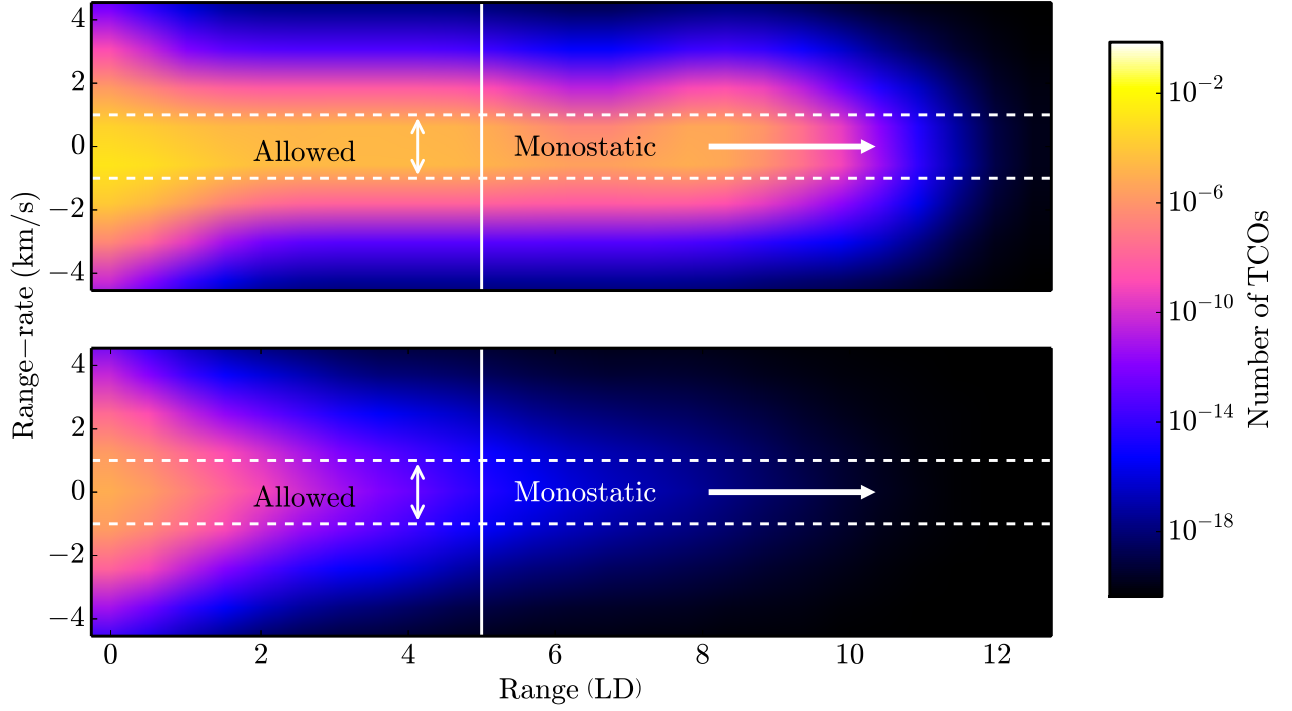


Fig. 10.— Range-rate vs. range distribution for TCOs in a 1° opening angle cone centered on the east and west quadratures. The top panel imposes no constraints on the objects’ detectability while the bottom panel incorporates the constraints on $S/N \geq 14$ and range-acceleration $< 10^{-4}$ cm/s (see fig. 11). The S/N requirement incorporates the effects of the TCOs’ rotation rates. The vertical solid line represents the minimum distance for which mono-static radar operations are possible with Arecibo. We restrict the range-rate of detectable TCOs to $[-1 \text{ km/s} : +1 \text{ km/s}]$ as indicated by the region between the two horizontal dotted lines.

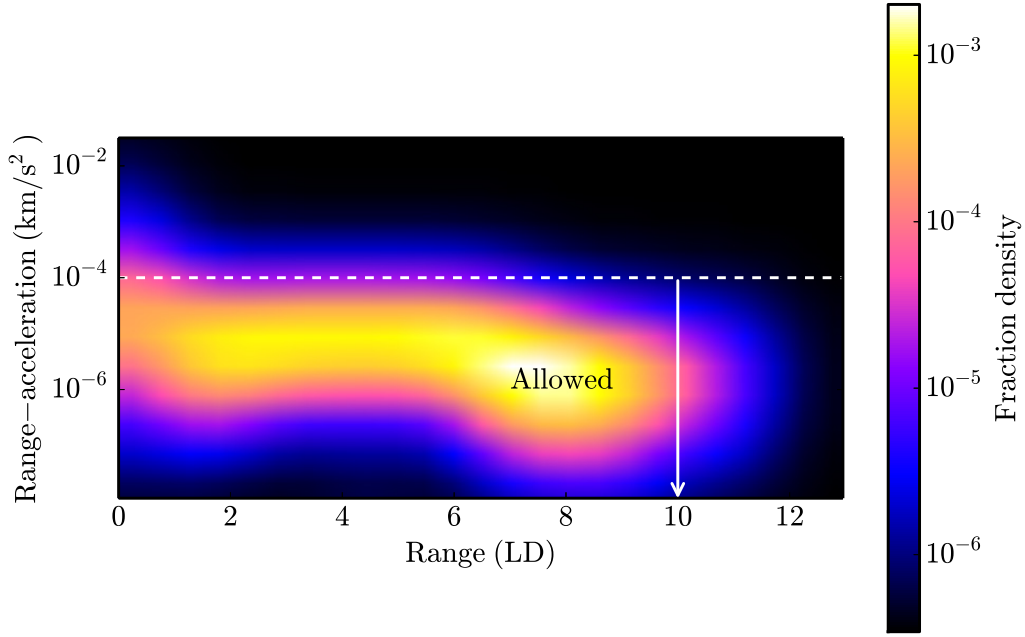


Fig. 11.— Range-acceleration ($\ddot{\Delta}$) vs range distribution for minimoons near the east and west quadratures. There is a steep rise in range-acceleration for minimoons at ranges of < 1 LD. More than 99% of TCOs are accelerating at $< 10^{-4}$ km/s⁻² as indicated by the dashed horizontal line. The number of objects in the $\ddot{\Delta}$ - Δ range, $(\ddot{\Delta} \pm d\ddot{\Delta}/2, \Delta \pm d\Delta/2)$, is the product of the fraction density and $(d\ddot{\Delta}, d\Delta)$.

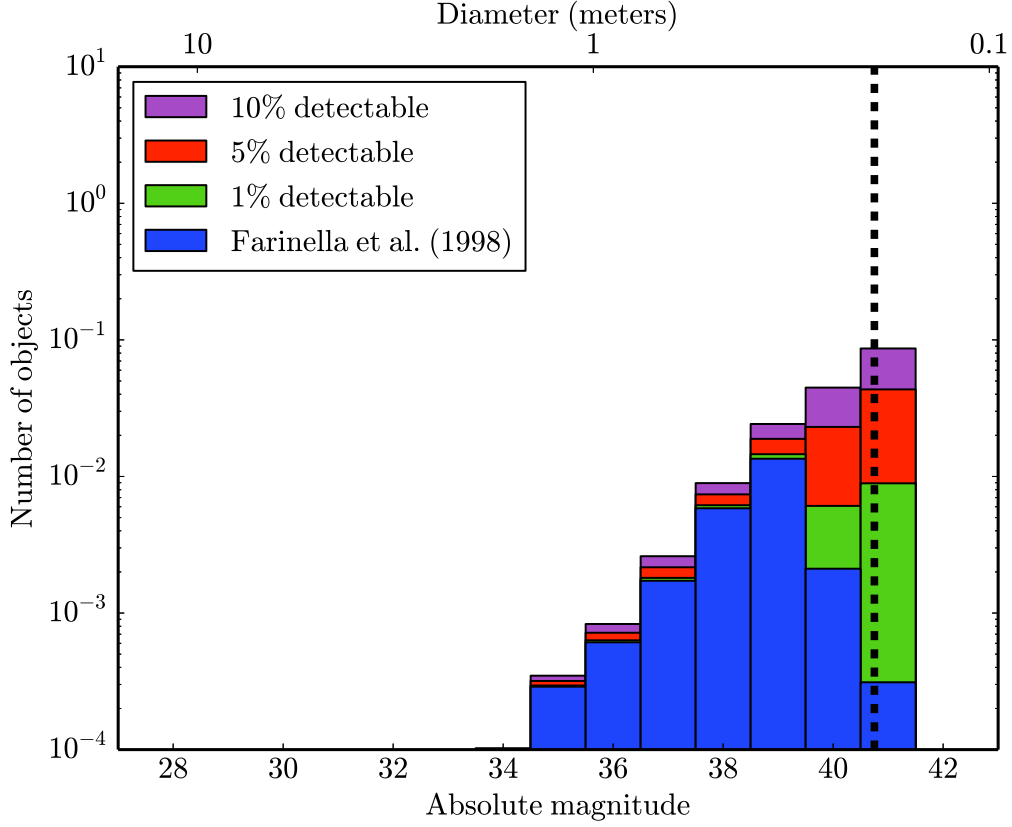


Fig. 12.— Size distribution for TCOs discovered in our simulations of bi-static radar operations with the Arecibo and Green Bank facilities. The four histograms represent different underlying rotation period distributions. The nominal distribution of Farinella *et al.* (1998), and 3 modified distributions that artificially increase the percentage of objects with detectable rotation periods to 1%, 5% and 10%. A dashed vertical line at 0.03m indicates where Rayleigh scattering prevents detections of small TCOs. *i.e.* all detections in the simulation with diameter ≤ 3 cm have been removed but we have not eliminated any detections with diameter > 3 cm.

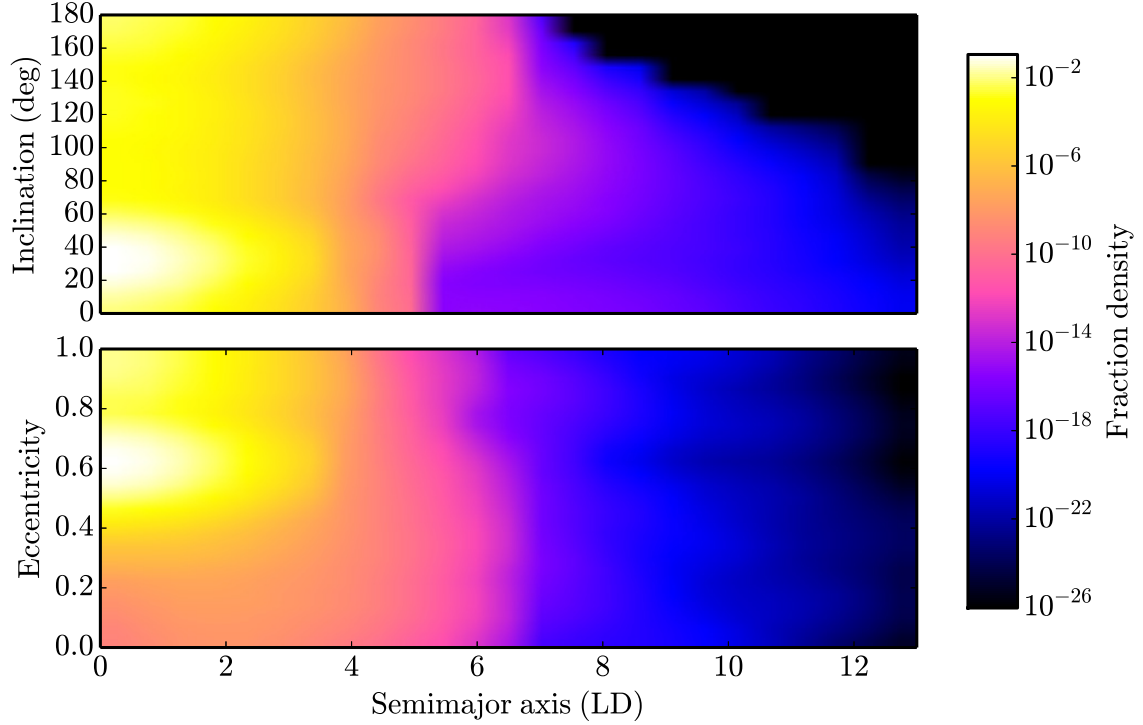


Fig. 13.— Geocentric semi-major axis vs. inclination (top) and eccentricity (bottom) distributions for minimoons discovered in our bi-static radar simulations in the direction of the quadratures. The distributions are dominated by TCOs with lifetimes $> 2,000$ d with inclinations of $\sim 40^\circ$ and moderate eccentricities of ~ 0.6 . Letting x represent either inclination or eccentricity, the number of objects in the x - a range, $(x \pm dx/2, a \pm da/2)$, is the product of the fraction density and (dx, da) .

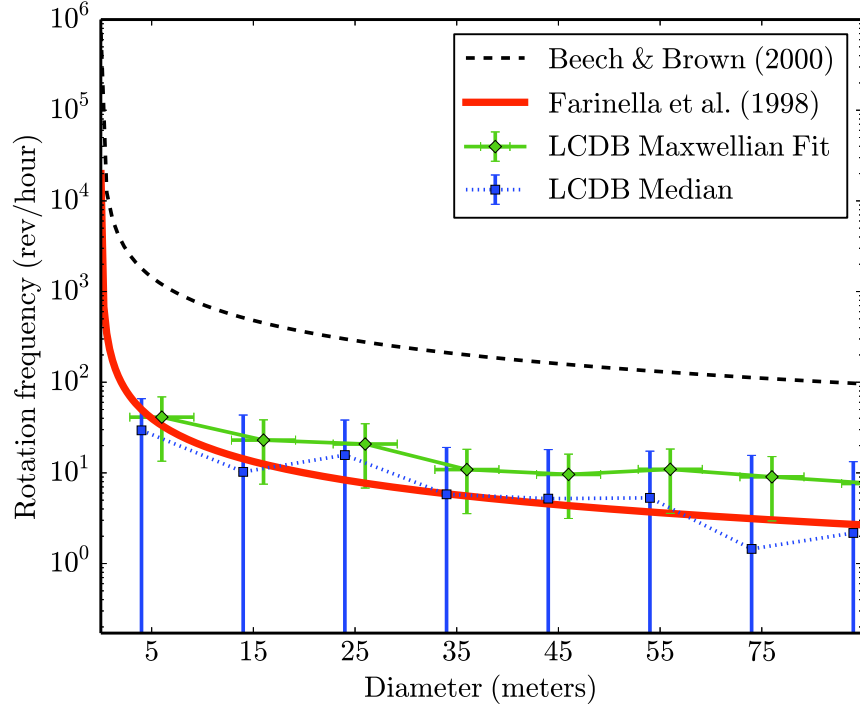


Fig. 14.— Rotation frequency of small asteroids as a function of diameter from (thick solid line) Farinella *et al.* (1998) and (dashed line) Beech and Brown (2000). The data points joined by dotted lines represent the median of the data in 10 meter diameter bins from the Light Curve Database (LCDB; Warner *et al.* 2009). The data points joined by thin solid lines represent our calculated median values from Maxwellian fits to the LCDB data in each bin. The LCDB data was combined in 10 m diameter bins and the data points are offset for the purpose of clarity by ± 1 m from the central values in each bin.